Article:
Evans, David, Gray, William R., Rae, James W.B. et al. (5 more authors) (2020) Trace and major element incorporation into amorphous calcium carbonate (ACC) precipitated from seawater. Geochimica et Cosmochimica Acta. pp. 293-311. ISSN: 0016-7037

https://doi.org/10.1016/j.gca.2020.08.034

Trace and major element incorporation into amorphous calcium carbonate (ACC) precipitated from seawater

David Evans[1*†], William R. Gray[1,2], James W. B. Rae[1], Rosanna Greenop[1], Paul B. Webb[3], Kirsty Penkman[4], Roland Kröger[5], & Nicola Allison[1]

[1] School of Earth and Environmental Sciences, University of St Andrews, St Andrews, UK
[2] Laboratoire des Sciences du Climat et de l'Environnement (LSCE/IPSL), Gif-sur-Yvette, France
[3] School of Chemistry, University of St Andrews, St Andrews, UK
[4] BioArCh, Department of Chemistry, University of York, York, UK
[5] Department of Physics, University of York, York, UK
* Now at: Institute for Geosciences, Goethe University Frankfurt, 60438 Frankfurt am Main, Germany
† evans@em.uni-frankfurt.de

Abstract

Amorphous calcium carbonate (ACC) has been identified or inferred to exist in many groups of marine organisms that produce biominerals widely used as geochemical archives (e.g. foraminifera, molluscs, echinoderms). However, little is known about trace element incorporation into ACC, and thus it is not understood how precipitation through an ACC precursor might impact the fidelity of climate proxies and biomineralisation models built on the skeletal geochemistry of these marine calcifiers. To address this, we investigated the incorporation of Li, B, Na, Mg, Mn, Sr, Ba, and U into inorganic amorphous calcium magnesium carbonates precipitated from seawater under a variety of different carbonate chemistries, Mg/Ca ratios, and in the presence of aspartic and glutamic acid, two of the most common intracrystalline amino acids found in foraminifera and corals. ACC is highly enriched in most of these trace elements relative to the crystalline carbonates yet similar in some respects in terms of the factors influencing trace element partitioning. For example, ACC B/Ca is sensitive to the carbonate system, whilst Mg/Ca and Sr/Ca are largely a function of their respective ratio in seawater. In general, we find that most of the variance in the distribution coefficients of the other trace elements can be explained by some combination of the seawater carbonate chemistry and the seawater or ACC Mg/Ca ratio.

1. Introduction

Geochemical proxies based on the (trace) elemental or isotopic composition of carbonate minerals are important tools for understanding past environmental changes. While such proxies are typically empirically calibrated, understanding the mechanistic basis of these techniques is key to identifying instances in which further calibration is necessary, or when existing calibrations may not be applicable. As such, knowledge of the geochemistry of ACC is required to understand how precipitation through an amorphous precursor might impact our understanding or interpretation of $CaCO_3$-hosted proxy systems, which form the basis of a substantial portion of our knowledge of palaeoceanography and palaeoclimatology.

In addition, much of our understanding of the biomineralisation process of calcifying marine organisms is derived from the comparison of skeletal chemical data to inorganically precipitated carbonates (Bentov and Erez, 2006; Gagnon et al., 2012; de Nooijer et al., 2014; Decarlo et al., 2018). These forward modelling exercises are based on elemental partition coefficients and isotopic fractionation factors into calcite and aragonite, which may enable the conditions at the calcification site to be reconstructed. For example, the inorganic calcite Mg distribution coefficient (D_{Mg}) is 1-2 orders of magnitude higher than the apparent D_{Mg} of planktonic foraminifera (Mucci and Morse, 1983; Bentov and Erez, 2006; De Choudens-Sanchez and Gonzalez, 2009). The most parsimonious explanation for this difference is that these organisms likely reduce the Mg/Ca ratio of their calcifying environment in order to produce low-Mg calcite (Erez, 2003; Evans et al., 2018), highlighting how a relatively simple comparison can form the basis of an important component of a calcification model. One of the fundamental assumptions made by this approach is that $CaCO_3$ precipitation by marine organisms is analogous to inorganic precipitation from a (semi)enclosed environment that is modified in its elemental and/or carbonate chemistry with respect to seawater. However, it has since been found, or inferred, that several major groups of marine calcifiers precipitate through an amorphous precursor phase (Beniash et al., 1997; Politi et al., 2006; Sviben et al., 2016; Jacob et al., 2017). This potentially poses a complication for the inference of calcification site conditions from skeletal geochemistry because little is known about the distribution coefficients of trace elements in amorphous calcium carbonate (ACC), so an important step is missing from current models. This is of particular concern because previous studies have shown that the chemistry of ACC differs greatly from crystalline $CaCO_3$. For example, ACC D_{Mg} is >2 times higher than calcite (Blue and Dove, 2015).

Knowledge of the ACC precursor phase is important because the transformation of ACC to crystalline $CaCO_3$ must take place in the (semi)closed environment of the calcification space. Depending on the ACC/seawater ratio at the calcification site, the composition of ACC has the potential to greatly impact the solution elemental chemistry during the transformation process, even if the ACC-calcite transformation can take place through a dissolution-reprecipitation reaction (Giuffre et al., 2015).

Assessing the sensitivity of proxy systems and biomineralisation models to precipitation through an ACC precursor is challenging because few studies of trace element incorporation into ACC exist. Furthermore, the geochemistry of ACC precipitated under conditions relevant to marine organisms has so far not been studied, i.e. from seawater rather than ionically simpler solutions. In order to address this, we present trace and major element data of amorphous carbonates precipitated from seawater-based solutions under a wide range of conditions, varying pH and DIC, the trace element/Ca ratio of seawater, the seawater [Mg^{2+}], and the concentration of two amino acids relevant to biomineralisation (aspartic and glutamic acid; Asp, Glu). Because seawater has a Mg/Ca ratio of 5.2, the samples discussed here are likely amorphous calcium magnesium carbonates rather than pure ACC. However, we use the term ACC throughout as amorphous carbonates precipitated from seawater have a Mg/Ca ratio <1, and there is no formal definition of the difference between these terms.

2. Materials & Methods

Four principal experiments were conducted: 1) A pH experiment, in which pH (8.95-10.36) and DIC (2.8-22.8 mM) broadly covaried as we were unable to produce ACC from (e.g.) low-pH, low-DIC seawater, 2) A seawater [Mg^{2+}] experiment, in which the Mg concentration was varied between ~0-50 mM at constant [Ca^{2+}], 3) A seawater [Ca^{2+}] experiment, in which the Ca concentration was varied between ~20-50 mM at constant [Mg^{2+}], and 4) An amino acid experiment, in which Asp and/or Glu were added up to a total concentration of 40 mM. This upper amino acid concentration is far in excess of that likely to be present at the calcification site of marine organisms (e.g. compare King and Hare (1972) and Kim et al. (2016)), which is extended here in order to better mechanistically understand the effect of the presence of these molecules. The precipitation dynamics of some of these experiments were previously described in Evans et al. (2019).

2.1 ACC precipitation and seawater carbonate chemistry

All experiments were conducted in artificial seawater (I = 0.72) made according to the recipe of Millero (2013) with the addition of several trace elements of interest at approximate open ocean concentrations (Li, Mn, Zn, Sr, Ba, the REE, and U), see the supplementary material. In some experiments the seawater Mg/Ca ratio was manipulated either by spiking 'normal' artificial seawater (Mg/Ca = 53/10.3 mM) with $CaCl_2$, or by spiking Mg-free artificial seawater with $MgCl_2$ (otherwise produced using the same recipe). Salinity was not adjusted in these experiments, such that it scaled with increasing [Ca^{2+}] up to 37 PSU (50 mM Ca^{2+}; I = 0.84) and decreasing [Mg^{2+}] down to 33 PSU (Mg-free seawater; I = 0.56). In the case of experiments conducted in the presence of amino acids, the desired amount of salt was weighed and added to the seawater immediately before the start of individual experiments. After the addition of the amino acid the solution was stirred vigorously for 10-15 minutes to ensure full dissolution, following which the carbonate system was readjusted to the desired conditions.

ACC was precipitated from seawater using a Metrohm 902 Titrando titrator as described in detail in Evans et al. (2019). In all cases precipitation took place in 250 ml of seawater placed into an acid-cleaned HDPE beaker (1 M HCl). Before every experiment the titrant dosing tubes and electrodes were cleaned in weak (0.1 M) HCl to ensure no residual precipitate from the previous titration. Prior to beginning the experiment, the seawater carbonate chemistry was adjusted close to the desired value by slowly pipetting 1 M Na_2CO_3 during rapid stirring, following which the pH was modified through NaOH or HCl addition, monitored using a calibrated pH electrode (using traceable NBS buffers). A calibrated Ca electrode (using seawaters with measured [Ca^{2+}]) was monitored throughout this time to ensure that no precipitation took place while the carbonate chemistry was being adjusted. Once the desired pH and DIC values were reached, ACC precipitation was induced by controlled simultaneous titration of 0.45 M $CaCl_2$ and Na_2CO_3 solutions, added in most cases at a rate of 0.5 ml min^{-1} (see Tab. 1), whilst slowly stirring the solution throughout the precipitation process. Seawater temperature was approximately equivalent to room temperature, varying by <1.2°C within a titration, with a mean±2SD of 22.5±2.1°C across all experiments. The seawater and precipitate were immediately separated at the end of the experiment by vacuum filtration using a 0.2 µm nylon membrane filter. The precipitate was thoroughly washed four times with trace element-grade ethanol, air-dried, and stored in acid-cleaned micro centrifuge tubes. Sub samples of the filtered seawater were taken for DIC

analysis (performed immediately, see Sec. 2.3) and elemental chemistry. The latter were acidified to 5% HNO_3 for storage in an acid-cleaned polypropylene centrifuge tube. All plastic used to store samples was pre-cleaned with 1 M HCl.

The experimental setup is designed such that precipitation did not take place immediately, but after a relatively small degree of titration. In order to relate the precipitate geochemistry to the precise solution chemistry conditions at the onset of ACC precipitation, rather than the seawater reservoir, the pH and $[Ca^{2+}]$ electrodes were used to monitor the evolution of the seawater chemistry through the titration. The DIC and $[Ca^{2+}]$ at the onset of precipitation were calculated based on the deviation of the electrode-derived $[Ca^{2+}]$ titration curve from that predicted if all titrated $CaCl_2$ remained in solution (see Evans et al. (2019) for a detailed explanation). For example, $[Ca^{2+}]$ at the onset of precipitation equals the initial seawater $[Ca^{2+}]$ plus the total titrated $CaCl_2$ at the point at which the titration curve diverged from predicted. The seawater trace element/Ca ratio at the onset of precipitation was calculated using the trace element concentrations of the seawater reservoir and the $[Ca^{2+}]$ at the onset of precipitation, and it was this ratio that was used to calculate trace element distribution coefficients. For example, $Mg/Ca_{sw} = [Mg^{2+}]_{initial}/([Ca^{2+}]_{initial} + [Ca^{2+}]_{titrated})$, such that $D_{Mg} = (Mg/Ca_{precipitate})/([Mg^{2+}]_{initial}/([Ca^{2+}]_{initial} + [Ca^{2+}]_{titrated}))$. Precipitation typically preceded for <7 minutes (Tab. S4), during which time the electrodes were monitored until the precipitate and seawater were separated. In the case of experiments that yielded ACC, the mean 4RSD variation in $[Ca^{2+}]$ between the initiation of precipitation and the end of the experiment was 1.6% (maximum within any given experiment 5%), which we do not consider a significant source of uncertainty in the calculation of the distribution coefficients reported here. For experiments resulting in ACC precipitation, seawater pH variation between the onset of precipitation and the end of the experiment was <0.03 units. Experiments dominantly yielding calcite were characterised by a wider variation in pH (typically <0.1 units) and $[Ca^{2+}]$; the data are presented for comparison but are not discussed or interpreted here.

The seawater saturation state at the onset of precipitation was derived from the calculated $[Ca^{2+}]$ and DIC values, and the measured pH at the relevant point in the titration, using co2sys (Lewis and Wallace, 1998) with the constants of Dickson and Millero (1987) and Dickson (1990). While several studies have investigated ACC and amorphous calcium magnesium carbonate (ACMC) solubility (e.g. Brecevic and Nielsen, 1989; Purgstaller et al., 2019), this work has demonstrated that the solubility of

ACMC is strongly dependent on the Mg concentration of the solid phase and other factors. Because experimental solubility data are not reported here, and given that it is not known how the composition of ACC precipitated from seawater might differ from previous studies in a way that might affect solubility, we report saturation state simply as the $[Ca^{2+}][CO_3^{2-}]$ product.

2.2 Precipitate characterisation

The type of material precipitated was assessed through Raman spectroscopy and attenuated total reflectance Fourier-transform infrared spectroscopy (ATR-FTIR), as ACC can be readily distinguished from the crystalline polymorphs of $CaCO_3$ using these techniques (e.g. Andersen and Brečević, 1991). Raman measurements were collected using a Horiba Jobin Yvon LabRam HR800 with a 50× long-working-distance objective lens, an excitation wavelength of 514 nm, beam diameter of 1 μm, and a spectral resolution of ~1.8 cm^{-1}. Samples were initially analysed with a low laser energy (1%), which was gradually increased to maximise signal/noise whilst ensuring no laser-induced alteration of the amorphous samples took place. All scans were performed 20×5 times, and no processing was applied except for a linear fluorescent baseline subtraction. ATR-FTIR spectra were collected using a Bruker Platinum ATR infrared spectrometer fitted with a TGS detector (see the supplementary material). A baseline measurement was performed before the analysis of every sample, measurements were performed at 1.4 cm^{-1} resolution with 32 scans. TGA-MS curves of some of the precipitates discussed here have been previously reported (see Evans et al., 2019).

Precipitates were analysed for their major/trace element/Ca ratios using an Agilent 7500a inductively coupled plasma mass spectrometer (ICPMS) in the StAiG laboratory, University of St Andrews. Because of the possibility of ACC spontaneously transforming into a crystalline carbonate in the centrifuge tubes in which the samples were stored (Konrad et al., 2016), the entire sample was first dissolved in weak (~0.1 M) HNO_3 without transfer to avoid possible preferential selection of crystalline $CaCO_3$ or ACC. Once fully dissolved, all samples were centrifuged to remove any shards of the membrane filter and the supernatant transferred to a clean centrifuge tube. Next, an aliquot from each of these centrifuged samples was diluted 30:1 in 0.5 M HNO_3 and analysed for its $[Mg^{2+} + Ca^{2+}]$. Once determined, a second aliquot of each sample was diluted to 1 mM $[Mg^{2+} + Ca^{2+}]$ and reanalysed for the following masses (m/z): ^{7}Li, ^{11}B, ^{23}Na, ^{25}Mg, ^{43}Ca, ^{48}Ca, ^{55}Mn, ^{88}Sr, ^{138}Ba, and ^{238}U. Blank and standard measurements were performed every fifth sample. Raw counts were converted into

element/Ca ratios via blank subtraction, ratioing to ^{43}Ca, and standardisation using a multi-element solution with the same [Ca^{2+}] of the samples and a trace element composition similar to low-Mg foraminiferal calcite. Accuracy and precision were assessed by repeat analysis of three in-house multi-element standards with trace element concentrations comparable to the samples. The only exception to this was Mg/Ca, which is 1-2 orders of magnitude higher in ACC compared to the crystalline $CaCO_3$ routinely analysed using this protocol. In order to confirm the linearity of the response of the mass spectrometer at the high Mg/Ca ratios of the ACC samples, one of the in-house standards was spiked with a single element ICPMS Mg standard to a calculated Mg/Ca ratio of 353 mmol/mol. Repeat measurement of this modified standard yielded a value 6% higher, which likely results from the extrapolation of the uncertainty in the primary standard to these relatively high Mg/Ca ratios. Nonetheless, the precision of repeat measurements of the high Mg/Ca standard was <1% such that we can precisely resolve relative differences between samples, although an uncertainty of 6% should be applied to our Mg/Ca data when comparing to other studies.

Based on 26 analyses of three in-house standards analysed over the same time interval as the samples (except in the case of Mg, see above), analytical precision was <5% for Li and B, ~1% for Na, Mg, Mn, and Sr, 20% for Ba, and 10% for U/Ca (2SD) based on the standard with the most similar element/Ca ratio to the samples. However, the concentration of Ba and U in ACC is much higher than these secondary standards, such that this is likely an overestimate of analytical reproducibility. To assess procedural reproducibility, powder splits of five ACC samples were analysed twice. The average difference between the two analyses was 6% for Li, 3% for B, 9% for Na, <2% for Mg, Mn, and Sr, 4% for Ba, and 3% for U/Ca, comparable to the long-term reproducibility of the measurements.

2.3 Seawater analysis and speciation calculations

Seawater samples were analysed for their DIC concentration immediately after each experiment to avoid equilibration with the atmosphere using a LI-7000 CO2 differential, non-dispersive, infrared gas analyser (Apollo SciTech AS-C3). Calibration was performed using a seawater standard (Dickson batch 141), and in-house Na_2CO_3 standards were used to confirm the linearity of the analyser at the relatively high DIC of our experimental seawaters (Evans et al., 2019). The precision of individual samples assessed by repeat (>6) injections was routinely <0.2%, however because the instrument was

not calibrated before every sample, we report a conservative estimate of accuracy of ±8% based on the long-term variability in the calibrations.

Selected seawater samples were analysed for their trace element concentrations on a Thermo Element 2 SF-ICPMS at the National Oceanography Centre, Southampton, UK. Samples were diluted 1:500 with 3% HNO_3 spiked with 5 ppb In as the internal standard. Calibration was performed via an eight-point calibration line spanning the range of sample concentrations. ^{7}Li, ^{11}B, ^{86}Sr, ^{138}Ba, and ^{238}U were measured in low resolution mode, whereas ^{24}Mg, ^{43}Ca, ^{44}Ca, and ^{55}Mn were measured in medium resolution mode. In order to avoid dilution error (if present) impacting the seawater data, sample-specific dilution factors were calculated using the seawater $[Ca^{2+}]$, which is 10.3 mM in the case of the reservoir seawaters, and can be calculated in the case of seawaters collected at the end of the experiment using the calibrated Ca ISE as described in Sec. 2.1 (reservoir $[TE]_{corrected} = [TE]_{measured} \times [Ca]_{calculated}/[Ca]_{measured}$). Precision was assessed based on a pooled standard deviation of repeat analysis of seawater samples from two different reservoirs, to provide an estimate of data quality based on a larger number of analyses. Analytical reproducibility was 6% for Li, 4% for B, 6% for Mn, 6% for Sr, 18% for Ba, and 5% for U/Ca, respectively (1SD).

The Mg/Ca ratio of the seawaters collected at the end of each experiment were determined using the Varian Vista Pro ICP-OES (axial) at the Edinburgh Earth Observatory, UK. Samples were diluted 1:50 with 3% HNO_3 with 1 ppm Y as the internal standard. Calibration was performed via a six-point calibration line with a range of Mg and Ca concentrations spanning that of the samples. Precision based on replicate analysis of the seawater reservoirs was 2% (2SD) for Mg/Ca. In order to identify whether seawater Mg/Ca remained constant during the experiments, the calculated Mg/Ca at the onset of precipitation was compared to the measured Mg/Ca ratio at the end of the experiment. These datasets are offset by 1% on average, demonstrating no significant change in seawater Mg/Ca, although individual experiments may be offset from expected values by up to 10%. Given that insufficient ACC was precipitated to significantly change the seawater [Mg] (Fig. S4), we interpret this variance as resulting from a combination of the precision of the Ca ion-selective electrode (ISE) in seawater, the precision of the ICP-OES data, and possible minor precipitation between collection and filtration of the seawater samples at the end of the experiment.

Over the course of the experiments, $CaCl_2$ and Na_2CO_3 titration was performed until sufficient precipitate for characterisation had been produced (10-40 mg). In order to assess (1) whether trace element uptake into ACC resulted in a lowering of the seawater concentration, and (2) to ensure no procedural contaminant was present, the composition of seawater at the start and end of six experiments was compared. Variations in the concentrations of all elements between the start and the end of the experiment were broadly comparable to analytical precision (Tab. S4), with the exception of Mn. Seawater [Mn] decreased during all experiments because the ACC D_{Mn} is high (Sec. 3.2), by ~30% on average with individual experiments characterised by a decrease of 8-75% (8-30% excluding one analysis). Our reported D_{Mn} should therefore be considered in the context of a ~20-30% decrease in the seawater [Mn] during the course of the titrations such that these represent a lower constraint of ACC D_{Mn} rather than the true values, and with some of the variance in the D_{Mn} data explicable through changes in [Mn] during titration. In the case of experiments dominantly yielding calcite, the variation in element/Ca ratios over the course of the titration was often much higher (up to 50%) because the dosing rate was typically lower than the precipitation rate in these experiments. The calculated distribution coefficients for these experiments should be viewed in this context (Tab. 1), although we stress that we do not interpret these data, which are presented only to give a sense of the extent to which they differ from ACC precipitated under comparable carbonate system conditions.

Aqueous speciation modelling and activity calculations were performed with PHREEQC (Parkhurst and Appelo, 1999) v3.6 using both the minteq.v4 and pitzer databases for comparison; minteq considers a wider variety of ion pairs whereas pitzer is more applicable to high ionic strength solutions such as seawater. The exception to the above was boron, for which speciation was calculated using the temperature, salinity, $[Ca^{2+}]$, and $[Mg^{2+}]$ dependent pK_B using the MyAMI model of Hain et al. (2015) assuming that $[B(OH)_3] + [B(OH)_4^-] = [B_T]$. While the PHREEQC speciation model indicates that 4-11% of B_T is present as the $CaB(OH)_4^+$ ion pair (average 6%) and 6-12% is present as the $MgB(OH)_4^+$ ion pair (average 10%), we do not account for this when discussing boron partitioning in order to facilitate direct comparison to the majority of previous studies.

Note that square brackets are used throughout to denote total concentration, e.g. [Ca2+] does not imply a speciation calculation has been performed. Activities, free ion concentrations, and speciation calculations are noted where relevant.

3. Results

3.1 Precipitate characteristics and precipitation dynamics

ACC precipitated from seawater is characteristically formed of spherical shaped aggregates of approximately 100 nm diameter (Fig. 1A,B). Raman and FTIR spectra of the majority of the precipitates discussed here display characteristic features of ACC, such as a lack of visible Raman lattice mode vibrations and wide ν_1 peak (carbonate symmetric stretch, see Fig. 1E), as well as ~20 weight% water of crystallisation as evidenced by TGA-MS (Evans et al., 2019). Based on spectroscopic features such as these, the lack of any resolvable crystal structure based on XRD data of similar samples (Evans et al., 2019), as well as the geochemical data (see below), the precipitation experiments yielded exclusively ACC in all but two cases. Specifically, those conducted at the extreme basic end of the carbonate chemistry space investigated here resulted in ACC-brucite mixtures, whilst samples precipitated from seawater with a Mg/Ca ratio <1 were calcite or calcite-ACC mixtures (Fig. 1C,D,F,G and the supplementary material).

The carbonate and seawater chemistry conditions at which precipitation took place are summarised in Fig. 2 and described in detail in Evans et al. (2019). Briefly, in seawater with an initial Mg/Ca ratio close to natural (53/10.3 mM), ACC precipitation takes place when the $[Ca^{2+}]/[CO_3^{2-}]$ is close to 1, i.e. $[CO_3^{2-}]$ = 10±2 mM (Fig. 2A). The addition of amino acids serves to inhibit ACC precipitation, which in our experimental setup is overcome by additional $CaCl_2$ titration, so that amino acid concentration broadly covaries with the seawater $[Ca^{2+}]$ at the onset of precipitation. The only investigated method by which we were able to reduce the $[CO_3^{2-}]$ necessary for precipitation substantially below 10 mM (conditions potentially more relevant to the calcification site of marine organisms), was to reduce the seawater Mg/Ca ratio (Fig. 2C). Nonetheless, we were unable to precipitate ACC within the pH and DIC range thought to characterise the tropical zooxanthellate corals (Allison et al., 2014; McCulloch et al., 2017), and our lowest pH experiments are at the upper end of estimates of the foraminifera calcification site (de Nooijer et al., 2009; Bentov et al., 2009). However, the carbonate chemistry of seawater was not exhaustively varied in tandem with the seawater Mg/Ca ratio, such that ACC precipitation under directly comparable conditions may be possible.

In all cases highly saturated conditions with respect to $CaCO_3$ minerals were required, ranging between $[Ca^{2+}][CO_3^{2-}]$ products of 100-200 (mM^2), equivalent to $\Omega_{calcite}$ of ~30-60. Based on the

307 rhodochrosite K_{sp} of Johnson (1982), all seawaters used here were undersaturated with respect to this
308 mineral. Based on the strontianite and witherite K_{sp} data from Busenberg & Plummer (1984) and
309 Busenberg & Plummer (1986) and Ba^{2+}, Sr^{2+}, and CO_3^{2-} activities derived from the PHREEQC pitzer
310 model as described above, then the seawater solutions of our experiments were undersaturated with
311 respect to witherite ($\Omega_{witherite}$ = 0.03-0.16) but oversaturated with respect to strontianite ($\Omega_{strontianite}$ =
312 3.7-19.7). As such, we cannot exclude the possibility that some Sr was incorporated into the
313 precipitates as strontianite rather than directly into ACC, although we note that the seawaters were far
314 more saturated with respect to $CaCO_3$ which may imply $CaCO_3$ precipitation rates far higher than that
315 of $SrCO_3$, such that it is likely that the Sr/Ca data reported here dominantly represent Sr incorporation
316 into ACC rather than the precipitates reflecting ACC-strontianite mixtures.
317
318 In the pH/DIC experiment, saturation state at the onset of precipitation is negatively correlated with
319 Mg/Ca_{sw} (Fig. 2C), which varied as different degrees of $CaCl_2$ titration were required to induced
320 precipitation. This was not the case in experiments in which the seawater initial Mg/Ca_{sw} was modified
321 by experimental design, which are characterised by an approximately constant saturation state with
322 decreasing Mg/Ca_{sw}.
323
324 **3.2 Precipitate trace element data**
325 Trace element/Ca ratios and apparent distribution coefficients (see Hauzer et al., 2018 for
326 terminology) of the precipitates were calculated as the element/Ca ratio in the solid relative to the
327 respective ratio in seawater ($[X/Ca_{ACC}]/[X/Ca_{sw}]$, where X denotes the total molar concentration of a
328 trace or major element), detailed in Tab. 1 and shown in Fig. 3 as a function of seawater pH, with
329 seawater-precipitate trace element/Ca relationships shown for comparison. We initially report
330 distribution coefficients relative to the total seawater element/Ca ratio for consistency and because we
331 have no *a priori* knowledge of which species are incorporated into ACC. In the discussion, we explore
332 the possibility that certain species are preferentially incorporated and/or partitioned into anion sites,
333 especially in the case of B and U. Data from experiments that yielded calcite or calcite-ACC mixtures
334 are also shown so that comparison may be made to crystalline samples precipitated under broadly
335 similar carbonate chemistry conditions. Of the precipitates with a crystalline component, endmember
336 experiments conducted at the lowest Mg/Ca_{sw} (~0.7 mol mol^{-1}) are likely almost entirely composed of
337 calcite and enable a sense of the difference between ACC and calcite to be ascertained when

precipitating using our experimental design. However, we do not discuss these data in detail because the precise ratio of calcite/ACC in these samples was not determined.

All ACC samples were thoroughly washed with ethanol prior to analysis (see Methods), however the absence of a minor seawater contaminant cannot be fully excluded. For the majority of the trace element data we report, the presence of minor amounts of seawater cannot significantly bias the data as most of these elements are present at a high concentration in ACC (e.g. Mg, Sr) or a low concentration in seawater (Mn, Ba, U). Li and Na/Ca ratios in any carbonate sample are sensitive to seawater contamination, although we do not observe the slope between Li/Ca and Na/Ca that would be expected if remnant seawater is the principal control on these trace elements (~1×10^{-4}, see Fig. S7).

***Lithium*:** The ACC Li distribution coefficient is low (~10^{-3} to 10^{-2}), with the implication that incorporation cannot be governed by the thickness of the diffusive boundary layer, i.e. the [Li] of the seawater layer around the ACC cannot be greatly modified through the process of precipitation, as very little Li is incorporated. ACC D_{Li} is comparable to the upper range reported for calcite (0.7-10.1×10^{-3} cf. 4×10^{-3} reported in Marriott et al., 2004). In seawater with a Mg/Ca ratio close to natural there is no significant relationship between D_{Li} and pH ($R^2 = 0.33$, $p = 0.07$), or between seawater-precipitate Li/Ca, when these variables are considered in isolation, in contrast to calcite (Okumura and Kitano, 1986; Füger et al., 2019). The presence of Asp or Glu at any concentration do not resolvably impact Li incorporation into ACC (Fig. 3B,C), and samples precipitated in low-Mg seawater are not offset from the others. Combining all of these experiments, D_{Li} in ACC is $1.3\pm0.8\times10^{-3}$ (2SD). Raising the seawater [Ca^{2+}] above 20 mM was the only investigated variable to result in an offset from the data described above; these experiments are characterised by more scattered Li/Ca values for a given pH, and a higher D_{Li} up to ~0.01. However, there is no systematic relationship between seawater-ACC Li/Ca (note that the seawater ratio was varied by changing the [Ca^{2+}]), at face value implying a lack of a true D_{Li} for ACC (but see discussion in Sec. 4.1).

***Boron*:** Boron incorporation in ACC is dominantly controlled by the carbonate system (Fig. 3D), as is well-known for the crystalline carbonates (e.g. Uchikawa et al., 2015a; DeCarlo et al., 2018), although the absolute B/Ca of ACC is ~2-4× higher than calcite precipitated here and previously reported. The presence of Asp and Glu do not significantly impact ACC B/Ca, and there is also no offset observed in

those precipitated from low-Mg seawater. There is also no systematic relationship between ACC and seawater B/Ca (Fig. 3F).

***Sodium*:** The ACC D_{Na} is similar to that of calcite precipitated under similar conditions (Fig. 3H), albeit ~2× higher than calcite and aragonite precipitated from ionically simpler solutions but similar solution Na/Ca ratios (White, 1977; Ishikawa and Ichikuni, 1984). There is no systematic relationship between Na/Ca or D_{Na} with pH or amino acid concentration. Within the variable seawater $[Ca^{2+}]$ experiments seawater and precipitate Na/Ca are correlated (Fig. 3I), indicating that there is a Na distribution coefficient into ACC, but the relationship is not statistically significant ($R^2 = 0.64$, $p = 0.06$) and the degree of scatter in the Na/Ca and D_{Na} data indicate that other factors impact Na incorporation.

***Magnesium*:** The Mg/Ca ratio of ACC precipitated from seawater with Mg/Ca close to natural is ~300-400 mmol/mol, ~4-5× higher than seeded overgrowth calcite precipitation in seawater (Mucci and Morse, 1983) and twice as high as calcite formed from ACC transformation in ionically simpler solutions (Blue et al., 2017). The relationship between seawater and ACC Mg/Ca is nonlinear, being best described by a power relationship:

$$Mg/Ca_{ACC} = 183\pm21\times Mg/Ca_{sw}^{0.58\pm0.09} \qquad \text{(eq. 1)}$$

$R^2 = 0.80$, $p << 0.01$, RMSE = 44 mmol mol^{-1} (coefficient uncertainties are 1SE). ACC is similar to calcite in this respect (Mucci and Morse, 1983), albeit with a marginally higher power coefficient (H = 0.4 for calcite). There is no relationship between D_{Mg} and pH (Fig. 3K), in contrast to calcite (Burton and Walter, 1991), although ACC precipitated at the extreme basic end of the investigated pH range (>10) are offset to Mg/Ca ratios ~100-200 mmol/mol higher. This most likely results from a minor brucite component in these samples (Fig. S1), and as such all experiments precipitated at a pH>10 are excluded from further discussion. Both the presence of both Asp and Glu in solution lower the Mg/Ca ratio of ACC (Fig. 3J), with the degree to which this is the case nonlinearly dependent on amino acid concentration (see Sec. 4.2).

***Manganese*:** Mn/Ca in ACC is positively correlated with pH in ACC precipitated from seawater with a Mg/Ca ratio close to natural (D_{Mn} increased with a slope of 27±4 per pH unit, Fig. 3M). Across all experiments, in some of which the $[Mg^{2+}]$ and/or $[Ca^{2+}]$ was varied by experimental design, a much

larger range (D_{Mn} = 20-200) was observed, similar to or slightly higher than that of calcite (Mucci, 1988). Nonetheless, we again stress that we do observe a decrease in the seawater [Mn] during the course of precipitation in our experiments (Sec. 2.2) such that these D_{Mn} are minimum values and some of the variance in the data is likely driven by possible differences in the amount of precipitation that took place between experiments. The addition of both Asp and Glu result in lower ACC Mn/Ca, but in contrast to Mg/Ca, the degree to which this is the case is amino acid dependent. For a given concentration, ACC precipitated in the presence of Asp has a lower Mn/Ca ratio compared to glutamic acid. Increasing the seawater [Ca^{2+}] resulted in higher Mn/Ca, and therefore a much higher D_{Mn}, despite the resulting lower seawater Mn/Ca ratios (Fig. 3M,N). Whilst not apparent from Fig. 3M,N,O, unlike most other trace elements, much of the variance in D_{Mn} described above can be explained by the seawater saturation state, discussed in detail in Sec. 4.1.

Strontium: We find no systematic relationship between ACC Sr/Ca and any parameter with the exception or Sr/Ca_{sw} (Fig. 3R). Unlike all of the other investigated trace elements, ACC-seawater Sr/Ca are linearly related irrespective of the seawater [Mg^{2+}] or amino acid concentration:

$$Sr/Ca_{ACC} = 0.67 \pm 0.02 \cdot Sr/Ca_{sw} \quad \text{(eq. 2)}$$

R^2 = 0.74, p <<0.01, RMSE = 0.65 mmol mol^{-1}. The ACC D_{Sr} is around three times higher than that of inorganic calcite (Mucci and Morse, 1983), but around half that of inorganic aragonite (Dietzel et al., 2004). The ACC Mg/Ca ratio does not impart a resolvable control on D_{Sr}, in contrast to calcite (Mucci and Morse, 1983), wherein lattice distortion resulting from Mg substitution for Ca is thought to result in increased Sr incorporation.

Barium: Like Sr, Ba/Ca is not characterised by a systematic relationship with pH, with a relatively invariant distribution coefficient of 1.82±0.27, around 20× higher than calcite (Kitano et al., 1971) but only marginally (1-2×) higher than that of inorganic aragonite (Dietzel et al., 2004; Mavromatis et al., 2018). There is also no systematic relationship between D_{Ba} and amino acid concentration. ACC precipitated from low-Mg seawater (10 mM) has a lower Ba/Ca ratio (Fig. 3T), D_{Ba} = 0.79±0.06. Experiments in high-Ca seawater result in ACC with similar Ba/Ca ratios (Fig. 3U), but higher distribution coefficients (driven by the denominator).

***Uranium*:** Uranium incorporation into ACC is unresolvably impacted by amino acid concentration, seawater [Mg^{2+}], or pH. Considering all three experimental sets together yields a constant D_U of 0.13±0.03 (Fig. 3W), with only ACC from the experiments performed in high-Ca seawater offset to higher U/Ca and D_U values. This is lower than inorganic aragonite (K_U = ~0.4 in the most highly saturated experiments of Decarlo et al. (2015)) but higher than that of calcite (K_U = 0.05 in the highest rate experiments of Weremeichik et al. (2017)). In aragonite the $UO_2(CO_3)_3^{4-}$ complex substitutes for $CaCO_3$, in contrast to calcite, wherein incorporation may occur via adsorption at step edges (Reeder et al., 2000; Reeder et al., 2004). ACC K_U alternatively calculated using the seawater U/CO_3^{2-} ratio reveals a positive relationship with pH in the subset of experiments conducted in seawater with the normal Mg/Ca ratio (m = 0.040, R^2 = 0.78, RMSE = 8.7×10^{-3}). However, we find no relationship between ACC U/Ca and the seawater U/CO_3^{2-} ratio.

The results above relate ACC element/Ca ratios to the respective total concentration ratio in seawater. This simple approach ignores that the free ion activity of all of the trace elements considered here is lower than the total concentration, but is useful because taking speciation or activity into account necessarily assumes something about the mechanism of incorporation. The results of the PHREEQC ion activity calculations are shown in Fig. 4 in comparison to the total concentration ratios for all amino acid-free experiments. This exercise demonstrates that total concentration ratios are linearly related to activity ratios in all cases, i.e. the dominant control on the activity ratios in these experimental seawaters is the concentration ratio, driven mostly by changes in [Ca^{2+}]. As such, uncertainty over which species are incorporated into ACC, as well as uncertainty in the speciation and activity calculations, cannot result in artefacts in the trends visible in Fig. 3 and in the more detailed discussion below. Calculating ACC (trace) element distribution coefficients using the activity ratios would result in values ~3 times higher in the case of Li and Na, whereas Mg/Ca and Sr/Ca activity ratios are not substantially different from their respective concentration ratios, such that the distribution coefficients described above and shown in Fig. 3 are not sensitive to alkali earth metal speciation in seawater. The minteq.v4 and pitzer databases predict α_{Ba}/α_{Ca} ratios that differ by ~50%, with the pitzer database, which is more applicable to high ionic strength solutions such as seawater, yielding a Ba/Ca activity ratio that would result in D_{Ba} ~27% lower than the concentration ratio. Mn/Ca activity ratios differ by an order of magnitude using the two databases, with the pitzer database resulting in α_{Mn}/α_{Ca} ratios ~7% lower than the concentration ratio. Considering seawater activity ratios

461 rather than concentration ratios would result in a linear transformation of the data to a good
462 approximation, and would only produce distribution that differ by <10% from those reported in Tab.1
463 except in the case of Li, Na, and Ba.
464
465 **4. Discussion**
466 **4.1 Growth rate and cation co-incorporation**
467 Precipitation rate is an important factor controlling trace element incorporation into the crystalline
468 carbonate minerals via (e.g.) surface entrapment(Watson, 2004; DePaolo, 2011). Whilst it is probable
469 that the same, or related, processes also impart an effect on trace element partitioning between
470 seawater and amorphous calcium carbonate, this is difficult to assess in our experiments because we
471 have no constraint on surface area-normalised ACC growth rate. Within the subset of 16 experiments
472 for which $[Mg^{2+}]$ was held constant at the natural value (53 mM) and no amino acids were added
473 (both factors are likely to influence precipitation rate), there is no relationship between seawater
474 saturation state and apparent distribution coefficient except in the case of D_{Mn} (Fig. S2), either
475 implying that growth rate is not important, that the $[Ca^{2+}][CO_3^{2-}]$ product is not a good proxy for
476 ACC growth rate, or that some other factor must also be considered. An argument against the first
477 two of these considerations is that there is a negative relationship between D_{Mn} and $[Ca^{2+}][CO_3^{2-}]$
478 which is also known for calcite (Mucci, 1988), implying that growth rate considerations are applicable
479 to ACC but masked by an additional factor in the case of Li, Ba, and U. Prime candidates are
480 competition between cations for incorporation into ACC, or that the composition of ACC itself may
481 impact the incorporation of other trace elements. For example, in the case of calcite, Mg substitution-
482 induced lattice distortion increases D_{Sr} (Mucci and Morse, 1983; Evans et al., 2015). Whilst a directly
483 analogous process cannot exist in amorphous materials, ACC has short-range order which is impacted
484 by its Mg/Ca ratio (Lam et al., 2007), and/or it may be that trace element distribution coefficients into
485 ACC are best described as the ratio to Ca+Mg given the overall high ACC Mg/Ca ratios (see the
486 supplementary material for an exploration of this). In either case the precipitate or seawater Mg/Ca
487 ratio could be an important consideration. There is no significant relationship between ACC Mg/Ca
488 and D_{Sr} (Fig. 5A), in contrast to calcite, whereas there is a strong effect of Mg/Ca on D_{Ba} (Fig. 5B). This
489 lends support either to the ACC Mg/Ca ratio imparting a control on the incorporation of some low
490 concentration trace elements for structural reasons, or to the notion that molar ratios in high-Mg
491 samples should be reported with Mg+Ca as the denominator (Fig. S7).

Given that both growth rate and the seawater or ACC Mg/Ca ratio are important controls on the incorporation of at least some low-concentration trace elements, multiple linear regression (MLR) analysis were performed on the 16 experiments at constant $[Mg^{2+}]$. As Mg/Ca in seawater and ACC are proportional to one another (Fig. 3L), we account for the possible impact of both seawater and precipitate Mg/Ca using the ACC Mg/Ca ratio using regressions of the form:

$$D_x = c + m_1 \cdot Mg/Ca_{ACC} + m_2 \cdot ([Ca^{2+}][CO_3^{2-}]) \quad \text{(eq. 3)}$$

Which assumes that seawater-ACC trace element/Ca ratios are linearly related through the origin. Regression models were produced for Li, Mn, Ba, U, the four trace elements for which there is clearly more than one dominant control on their incorporation into ACC (Fig. 3C,O,U,X). All four models are highly significant; R^2 range between 0.73-0.84, $p<<0.01$, RMSE/intercept ratios = 4-5% (Tab. S1), implying that these trace elements do in fact have an approximately linear distribution coefficient in ACC, overprinted in our experiments by the effect of ACC Mg/Ca and seawater saturation state. Both of these secondary factors are significant predictors in all models except in the case of D_{Mn}, which can be well-modelled by saturation state alone. That is, most of the variance in the observed trace element/Ca ratios can be ascribed to some combination of the seawater element/Ca ratio, saturation state, and the seawater or ACC Mg/Ca ratio. Whilst this also suggests ACC growth rate is linked to saturation state we stress that, in the absence of direct observational evidence for this, a causal link between saturation state and trace element incorporation via a presumed growth rate effect should be interpreted with caution.

If the saturation state effect predicted by these models is best attributed to growth rate, then an alternative formulation of this factor might be appropriate given that, in the case of calcite, growth rate is a function of the solution $[Ca^{2+}]/[CO_3^{2-}]$ ratio at constant Ω_c (Nehrke et al., 2007; Wolthers et al., 2012). In order to explore this, we repeat the MLR exercise with the saturation state parameter alternatively formulated as $[Ca^{2+}][CO_3^{2-}]/([Ca^{2+}]+[CO_3^{2-}])$. This accounts for an imbalanced $[Ca^{2+}]/[CO_3^{2-}]$ ratio in the denominator and is therefore more likely to be representative of growth rate (e.g. at constant Ω, 2+50 mM is larger than 10+10 mM, in-line with lower rates at ratios further from unity). These models result in slightly better fits to the data (RMSE reduced by ~15-40% compared to Eq. 3) and result in greater importance being assigned to this metric of growth rate and less importance to the ACC Mg/Ca ratio as predictors of D_x (see the supplementary material). This

suggests that the [Ca^{2+}] [CO_3^{2-}] product/sum ratio may be a better metric for growth rate where this cannot be readily independently assessed (e.g. via surface area measurement). For the purposes of the discussion here, it stands that some combination of saturation state/rate, Mg/Ca, and seawater element/Ca ratio results in model RMSE similar in magnitude to analytical precision, however the MLR models are formulated.

Pertinently, the MLR analysis of D_U is better able to explain the dataset when D_U is formulated relative to U/Ca_{sw} rather than the U/CO_3^{2-} ratio. This points towards an ACC U incorporation mechanism wherein $UO_2(CO_3)_3^{4-}$ is not the only species incorporated into ACC, in contrast to aragonite (Reeder et al., 2000). Alternatively, it may be that the majority of U_T is in the form of $UO_2(CO_3)_3^{4-}$ in all of our experiments such that the exact seawater [CO_3^{2-}] exerts little control on the concentration of the $UO_2(CO_3)_3^{4-}$ complex (see Keul et al., 2013). Whilst the latter hypothesis can explain the poorer performance of the D_U model that uses seawater U/CO_3^{2-}, it cannot explain the better performance of the model utilising U/Ca_{sw}. Like the other trace elements discussed above, ACC D_U is clearly tightly related to seawater chemistry in our experiments, although further work is required to better understand the exact mechanism of incorporation.

The range of ACC D_x are summarised in Fig. 6 and compared to selected published calcite data (Kitano et al., 1971; White, 1978; Mucci and Morse, 1983; Okumura and Kitano, 1986; Mucci, 1988; Marriott et al., 2004; Uchikawa et al., 2015; Weremeichik et al., 2017). ACC trace element distribution coefficients are 5-100 times higher than in calcite on average, with the exception of D_{Mn}, which is similar in both materials, and D_{Li}, for which the upper end of the calcite range overlaps with ACC. As with our ACC samples, a wide range in calcite distribution coefficients have been reported, driven by factors such as precipitation rate and the Mg/Ca ratio of the solid phase. Therefore, the size of the boxes in Fig. 6 represents the observed variance in distribution coefficients driven by environmental parameters, not uncertainty in the comparison. Moreover, it is likely that many of these factors drive both ACC and calcite distribution coefficients in the same direction. For example, increasing the [$B(OH)_4^-$]/DIC ratio results in higher B/Ca ratios in both materials. The intersection of the fields in Fig. 6B with the 1:1 line do not imply that the calcite and ACC distribution coefficients are within range of each other.

554 **4.2 Factors affecting boron and magnesium incorporation into ACC**

555 In Sec. 4.1 (and Fig. 3) we demonstrate that Sr and the low concentration trace elements have an
556 approximately constant distribution coefficient into ACC, which may be modulated by the seawater
557 and/or ACC Mg/Ca ratio, and seawater saturation state. Here we examine the controls on B and Mg
558 incorporation in detail given their importance as proxy systems and because their incorporation is
559 also dependent on other factors beyond those discussed above.

560

561 ***Boron*:** ACC B/Ca principally depends on seawater pH (Fig. 7A), irrespective of the seawater [Mg^{2+}],
562 [Ca^{2+}], or amino acid concentration. At face value, this suggests that the incorporation mechanism of
563 boron into ACC is relatively simple. If it is the negatively charged $B(OH)_4^-$ that is incorporated into
564 ACC, then the mechanistic basis for this relationship should be rooted in the pH-dependent seawater
565 [$B(OH)_4^-$] or [$B(OH)_4^-$]/DIC ratio (or similar, e.g. [$B(OH)_4^-$]/[HCO_3^-+CO_3^{2-}]), as previously observed
566 for calcite and aragonite (Uchikawa et al., 2015; Holcomb et al., 2016). This is indeed the case for
567 experiments precipitated from seawater with a Mg/Ca ratio close to natural (Fig. 7B), yet because
568 increasing the seawater [Ca^{2+}] enabled ACC precipitation at a greatly reduced DIC and [CO_3^{2-}], the
569 variable seawater [Ca^{2+}] experiments do not conform to a B/Ca-[$B(OH)_4^-$]/DIC relationship.
570 Assuming both $B(OH)_3$ and $B(OH)_4^-$ are incorporated into ACC – i.e. regressing against the total
571 seawater boron (B_T)/DIC ratio – yields a similar result (Fig. 7C), again because the total boron
572 concentration was held constant whilst DIC was reduced in the elevated [Ca^{2+}] experiments. For a
573 similar reason we are not able to identify which boron species (or combination thereof) are
574 incorporated into ACC, because pH and DIC unavoidably covaried in the carbonate chemistry
575 experiments (Fig. 2). That is, the tight relationship between ACC B/Ca and [$B(OH)_4^-$]/DIC (Fig. 7B)
576 could be driven either by increasing [$B(OH)_4^-$] and/or decreasing DIC relative to B_T. The relatively
577 narrow range in [CO_3^{2-}] between the experiments in seawater with the natural Mg/Ca ratio (Fig. 2)
578 means that whilst the $B(OH)_4^-/CO_3^{2-}$ ratio might be an additional driver of ACC B/Ca, it cannot be an
579 alternative explanation for the relationships shown in Fig. 7 (Fig. S5). Likewise, $B(OH)_4^-$ activity is
580 directly proportional to [$B(OH)_4^-$] calculated assuming the sum of the two major boron species in
581 seawater equals [B_T] (which is how the data are displayed in Fig. 7, see Sec. 2.3), with $\gamma_{B(OH)4-} = 0.32$.
582 While the abundance of the $CaB(OH)_4^+$ and $MgB(OH)_4^+$ ion pairs do vary in seawaters with
583 manipulated [Ca^{2+}] or [Mg^{2+}] (Fig. S6, $\gamma_{B(OH)4-}$ ranges between 0.26-0.39), the magnitude of this effect is
584 far too small to drive the trends discussed above (see Fig. S6).

An alternative possibility is that ACC B/Ca could be driven by the seawater $[B(OH)_4^-]$ alone, given that ACC precipitated from seawater with an elevated $[Ca^{2+}]$ lie on the same pH-B/Ca line as all other experiments (Fig. 7A), i.e. the discrepancy described above could be an artefact of normalisation to DIC. However, the asymptote of the seawater $[B(OH)_4^-]$-pH curve is approached above pH ~9.5, yet there is no reduction in the slope of the B/Ca-pH relationship above this pH. As such ACC B/Ca is not correlated with $[B(OH)_4^-]$ above pH ~9.5, and so $[B(OH)_4^-]$ alone also cannot explain the data. One solution to this issue is to regress the B/Ca data against $[B(OH)_4^-]$/DIC further normalised to the seawater $[Ca^{2+}]$ (Fig. 7D). Doing so causes B/Ca to collapse onto a single slope, albeit with a reduced goodness of fit compared to the B/Ca-$[B(OH)_4^-]$/DIC regression through the samples precipitated with a seawater $[Ca^{2+}]$ close to natural (RMSE = 116 and 95 respectively), although this is in-line with the relatively large x-axis uncertainties from the propagated Ca, DIC, and pH estimations. Because the seawater saturation state did not scale with seawater $[Ca^{2+}]$ (as increasing $[Ca^{2+}]$ resulted in a broadly proportionally lower $[CO_3^{2-}]$ required for precipitation, Fig. 2C), this normalisation is not necessarily a growth rate correction (see discussion of saturation state versus the $[Ca^{2+}][CO_3^{2-}]$ product/sum ratio as metrics of growth rate in Sec. 4.1). Fully resolving the mechanistic basis for boron incorporation into ACC is beyond the scope of this study, with possible additional considerations being a change in the characteristics of the growing ACC surface (Branson, 2018), or complex formation between Ca^{2+} and $B(OH)_4^-$ at high calcium concentrations. In any case it is encouraging for boron-based proxies that B incorporation into ACC is strongly sensitive to seawater carbonate chemistry (Fig. 7A), such that precipitation through an amorphous precursor is not necessarily a complication for boron-based proxies.

Magnesium: ACC Mg/Ca is predominantly, nonlinearly, controlled by the seawater Mg/Ca ratio. Figure 7 compares our Mg/Ca data to ACC precipitated at higher Mg/Ca ratios from non-seawater solutions (Blue and Dove, 2015), calcite precipitated from seawater (Mucci and Morse, 1983) and calcite formed from the transformation of ACC (Blue et al., 2017). Our data are in agreement with previous work in that we find ACC Mg/Ca far exceeds that of calcite precipitated under an equivalent Mg/Ca ratio (Blue and Dove, 2015). However, unlike Blue and Dove (2015) we find no resolvable pH dependency of ACC Mg/Ca (Fig. 3K). The reasons for this may stem from the different experimental design, most notably that we precipitate ACC from seawater rather than $MgCl_2$-$CaCl_2$-$NaHCO_3$ solutions. Whatever the cause for the pH dependency that has been previously reported, our results

indicate that it may not be manifest when precipitating from seawater, especially at biologically relevant pH.

As previously described (Wang et al., 2009), the presence of high concentrations of carboxylated molecules that form ligands with Ca and Mg in solution can impact the Mg/Ca ratio of ACC. The basis for this lies in the differential affinity that these molecules have to form ligands with Mg^{2+} and Ca^{2+}, thereby impacting the free Mg^{2+}/Ca^{2+} ratio. Precipitation in the presence of molecules such as Asp should result in a lower ACC Mg/Ca ratio, as this molecule has a preferential affinity to form ligands with Mg^{2+} over Ca^{2+} in solution. Consistent with this model, we find that ACC precipitation from seawater containing Asp and Glu results in a lower ACC Mg/Ca (Fig. 9) according to a power relationship, with the effect of Asp and Glu being indistinguishable from one another. Increasing the concentration between 2 to 10 mM resulted in ACC with a Mg/Ca ratio ~40% lower than the average of the amino acid-free experiments (290 cf. 425 mmol mol^{-1}; Fig. 9), whilst further increase up to an amino acid concentration of 40 mM resulted in only a minor further reduction in ACC Mg/Ca to 240 mmol mol^{-1}. This is in contrast to the results of Wang et al. (2009), wherein ACC precipitated in the presence of Asp had a higher Mg/Ca ratio than the biomolecule free control experiment, possibly pointing an additional complicating factor in those experiments. Moreover, the data of Wang et al. (2009) are characterised by a positive relationship between amino acid concentration and ACC Mg/Ca ratio, in contrast to our results and despite the preferential affinity of these molecules to form ligands with Mg^{2+}. One key difference between Wang et al. (2009) and this study is that our samples were precipitated from seawater under tightly controlled carbonate system conditions, such that it may be that ion-pairing and formation of ligands in more complicated solutions such as seawater alters the resulting chemical characteristics of ACC. Whatever the cause, this difference highlights the importance of precipitating ACC under conditions that are as relevant as possible to the system of interest.

5. Conclusion

The systematics of trace element partitioning between seawater and ACC were investigated under a variety of different carbonate system conditions and element/Ca seawater ratios (principally by varying $[Ca^{2+}]$). Data for many of the most commonly studied trace elements with respect to proxy systems in biogenic carbonate archives and biomineralisation models are presented (Li, B, Na, Mg,

Mn, Sr, Ba, U). Several aspects of trace element incorporation into ACC are similar to the seawater-calcite system, e.g. B/Ca is strongly a function of the carbonate system, the seawater-ACC Mg/Ca response is characterised by a power relationship, and Sr has an approximately constant distribution coefficient. In general, trace elements characterised by distribution coefficients lower than one in calcite also have D_x <1 in ACC, although Ba is an exception, and the D_x of all trace elements is ~1-2 order of magnitude higher in ACC than calcite, with the exception of Mn (similar for both materials). Unlike calcite, where the solid Mg/Ca ratio imparts a control on D_{Sr} probably through lattice distortion, there is no relationship between ACC Mg/Ca and D_{Sr}. D_{Ba} is negatively correlated with the ACC Mg/Ca ratio, possibly suggesting that low concentration divalent ions are incorporated to a higher degree when ACC contains less Mg, or that trace element ratios should be reported relative to Mg+Ca in high-Mg samples. Finally, we find that high concentrations (>5 mM) of both Asp and Glu strongly inhibit Mg incorporation into ACC, in contrast with a previous study but as predicted by changes in the Mg/Ca activity ratio as a result of the differential binding constants these organic molecules have to form ligands with Mg^{2+} and Ca^{2+} in solution. The only other trace element resolvably impacted by these amino acids was Mn, with ACC precipitated in the presence of both Asp and Glu characterised by lower D_{Mn}.

Acknowledgments. We are grateful to Laetitia Pichevin and Matthew Cooper for help with the seawater ICP-OES and ICP-MS analyses, respectively, and we are indebted to Jonathan Erez for many stimulating discussions. We would like to sincerely thank the editor and three anonymous reviewers whose comments substantially improved this contribution. This work was supported by the Leverhulme Trust (Research Project Grant 2015-268 to NA, RK, and KP).

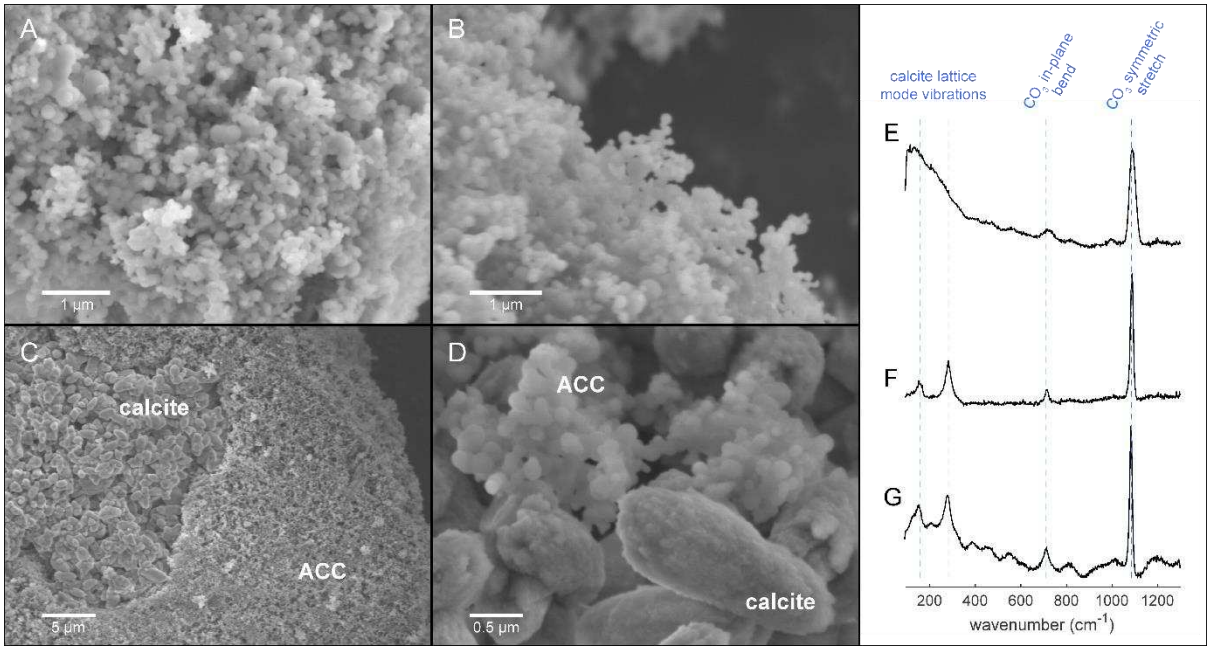

Fig. 1. Representative SEM images (A-D) and Raman spectra (E-G) of the precipitates discussed here. (A) ACC precipitated from seawater with the natural Mg/Ca ratio of 5 at pH ~10. (B) ACC precipitated from low-Mg seawater (15 mM) at pH ~9.5. (C) Precipitate resulting from seawater with [Ca^{2+}] increased to result in Mg/Ca_{sw} <1 at pH ~9.5. Two distinct components are present, ACC and calcite (identified through Raman and FTIR spectroscopy). (D) As in panel C except precipitated at pH ~10. Crystalline $CaCO_3$ particles are evident. Note panels C & D are shown for illustrative purposes, calcite was not detectable in most precipitates. (E) Representative Raman spectra of ACC precipitated from seawater with the natural Mg/Ca ratio. The lack of discernible lattice-mode vibrations and the wide ν_1 peak (CO_3 symmetric stretch) demonstrate the amorphous nature of this material (also see Fig. S1). (F) Raman spectra of the precipitate resulting from seawater with a Mg/Ca ratio <1 at pH 9.5. Lattice-mode vibrations indicate the presence of calcite, whilst the asymmetric ν_1 peak is consistent with the presence of both calcite and ACC (Evans et al., 2019) as also observed via SEM imaging. (G) At Mg/Ca_{sw} <1 and pH 10 calcite lattice-mode vibrations are visible albeit less well-defined, again indicating the presence of both ACC and calcite.

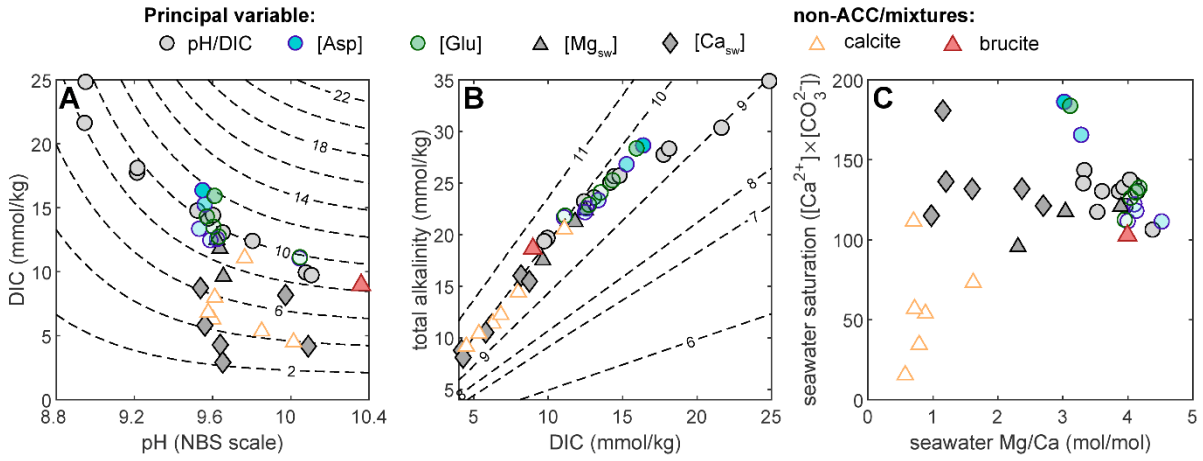

Fig. 2. The seawater chemistry conditions under which ACC and other materials were precipitated. (A) pH-DIC with [CO_3^{2-}] shown by contours. ACCs precipitated from seawater with Mg/Ca close to the natural ratio of ~5 (circles) all fall within ±2 mM of the 10 mM [CO_3^{2-}] line. Reducing Mg/Ca_{sw} either through lowering Mg^{2+} or raising Ca^{2+} was the only mechanism investigated here by which the seawater DIC necessary for ACC precipitation could be substantially reduced. Amino acid concentration is shown as a function of symbol opacity (solid colours represent the highest concentration, 40 mM). (B) The location of the experiments in alkalinity-DIC space, with pH shown by contours. (C) The seawater carbonate mineral saturation state ([Ca^{2+}][CO_3^{2-}]) at the onset of precipitation as a function of the seawater Mg/Ca ratio. In most cases the resulting precipitate was ACC, with the exception of (1) seawater with a Mg/Ca ratio ≤~1 mol/mol, which resulted in calcite or calcite-ACC mixtures (see Fig. 1), and (2) at the extreme basic end of the pH range investigated (>10), which resulted in ACC-amorphous brucite mixtures. [CO_3^{2-}] and total alkalinity were calculated from pH and DIC using co2sys (Lewis and Wallace, 1998).

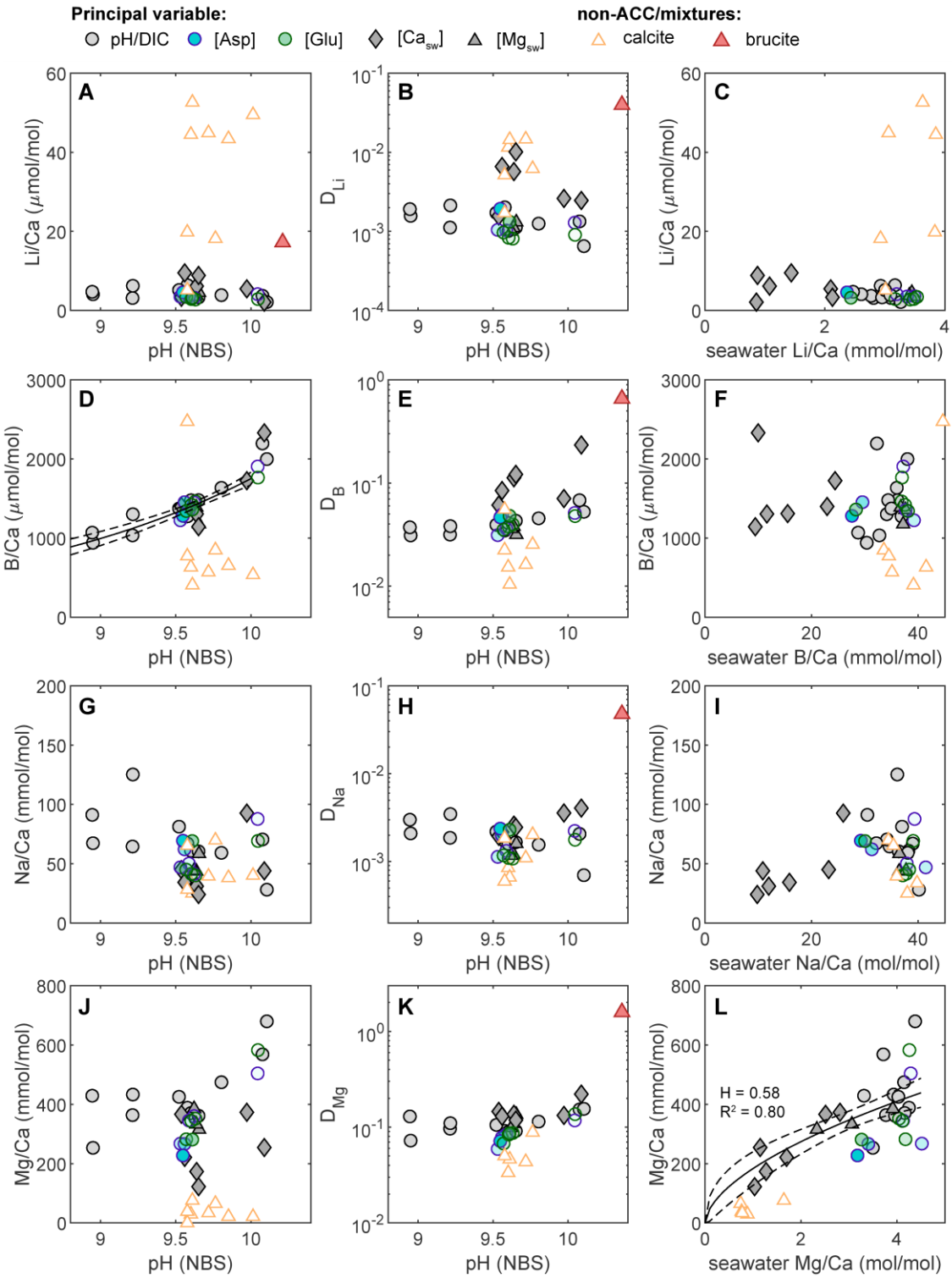

Fig. 3. Overview of trace and major element incorporation into ACC precipitated from seawater as a function of pH (left, centre) and the seawater element/Ca ratio (right). In the case of pH, both the precipitate element/Ca ratio (left) and distribution coefficient (centre) are shown as the method used to precipitate ACC meant that the seawater [Ca^{2+}] was not identical in all cases (see methods). Calcites and/or calcite-ACC mixtures precipitated under similar carbonate chemistry conditions and an amorphous brucite-ACC mixture are shown for comparison. Note that the latter is omitted from some plots to avoid scale compression, and that the scatter in the 'calcite' data arises because some samples are calcite and some are mixtures based on their Raman spectra.

See Fig. S7 for the data replotted as the ratio to Ca+Mg, in order to account for the high mole% Mg of these ACCs,

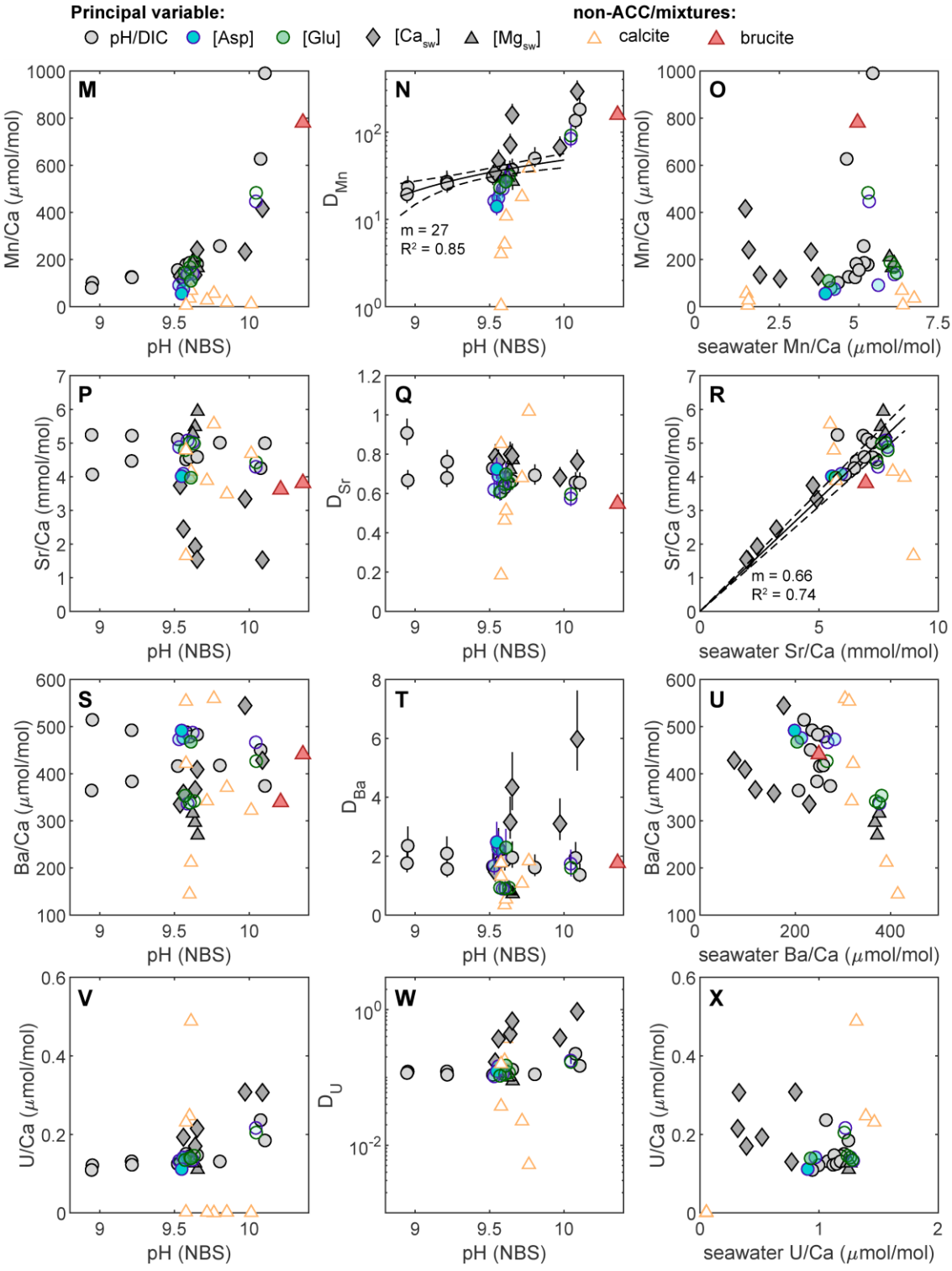

Fig. 3. Cont.

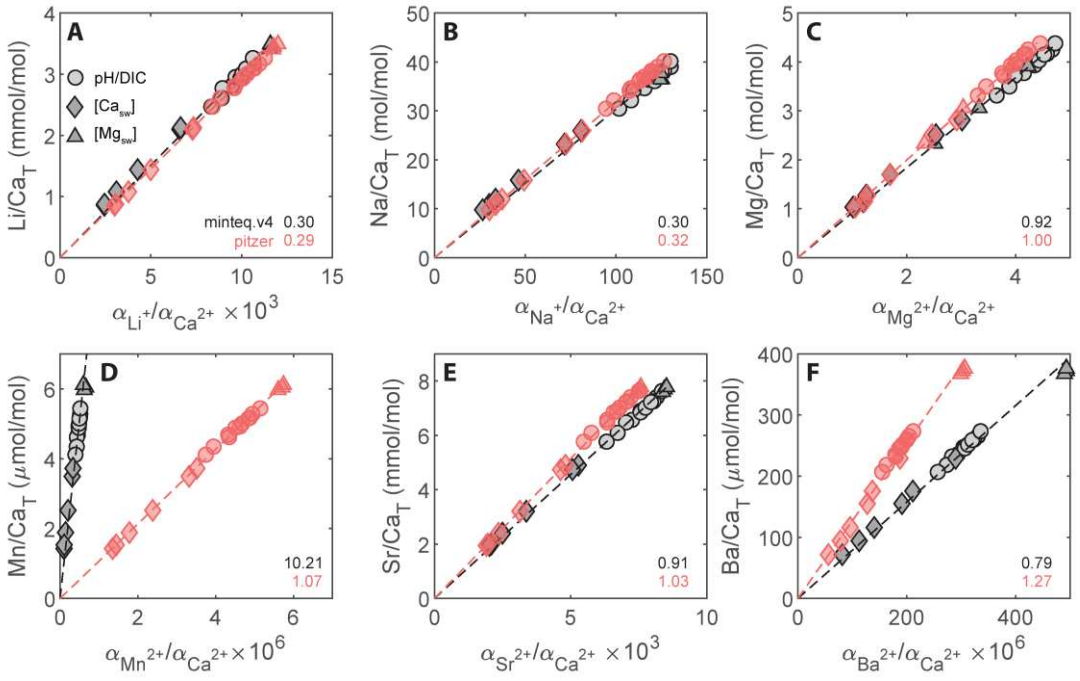

Fig. 4. The relationship between the ion activity ratios and total concentration ratios for the amino acid-free experiments presented here, calculated using PHREEQC with both the minteq.v4 and pitzer databases. We note that the application of the minteq.v4 database to high ionic strength solutions is not necessarily recommended and is presented here only for comparison. Importantly, the activity-concentration ratio relationship is linear to a good approximation (slopes given in the lower left corner of each panel), that is, changes in the activity ratio are principally driven by changes in [Ca] rather than pH, DIC, etc.

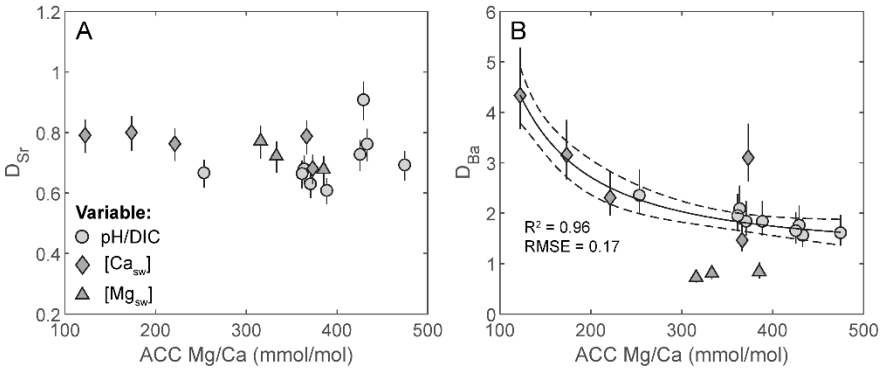

Fig. 5. Investigating the role of seawater and/or ACC Mg/Ca on the co-incorporation of other alkali earth metals. (A) There is no relationship between ACC Mg/Ca and D_{Sr}, differentiating ACC from calcite in this respect (Mucci and Morse, 1983). (B) In contrast, Mg/Ca may exert a strong control on D_{Ba}, possibly implying competition between Mg^{2+} and the low-concentration divalent metal ions. One outlier (based on its Cook's distance), and the low-Mg seawater data are excluded from the regression. The overall nonconformity of these latter data, and the factor of two lower D_{Ba} in low-Mg seawater implies that both seawater and precipitate major ion chemistry influence ACC Ba incorporation.

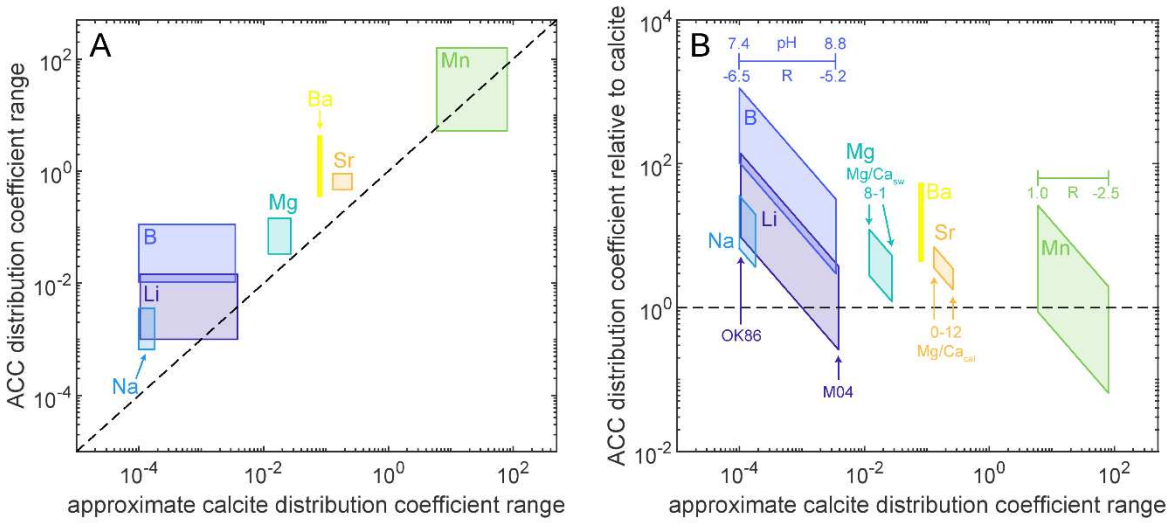

Fig. 6. (A) Major and trace element distribution coefficients in ACC precipitated from seawater (this study) compared to calcite. The heights of the boxes are equal to the range of ACC distribution coefficients found under the different seawater chemistries investigated here, which is an indication of the extent to which the distribution coefficient depends on boundary conditions and not an estimate of uncertainty. The widths of the boxes represent the range of distribution coefficients either within or between calcite studies (more than one study has been conducted in the case of Li and Na). Where possible, only data from calcite experimentally precipitated in seawater were used (Mg, Sr only). Note that (e.g.) the narrow width of the Ba box may reflect the limited amount of research on Ba incorporation into calcite. (B) The ACC distribution coefficients alternatively displayed relative to the respective calcite values. In general, ACC trace element distribution coefficients are ~5-100 times higher than calcite with the exception of Mn (but note that we constrain the minimum ACC D_{Mn} of the experiments presented here, true values may be ~30% higher, see Sec. 2.2). The principal experimental variables of the calcite studies (growth rate, pH, Mg/Ca_{sw}), or the location of certain studies (in the case of Li) are labelled. Note that processes that result in a change in the calcite distribution coefficient for a certain trace element may exert a similar control on the respective ACC distribution coefficient, e.g. increasing pH results in higher B/Ca ratios in both calcite and ACC. In these cases, the data would be more appropriately displayed using a (sub)horizontal line, but we do not do so in the absence of directly comparable calcite and ACC experiments in terms of solution chemistry and experimental design. OK86 and M04 refers to Okumura and Kitano (1986) and Marriott et al. (2004) respectively, see Sec. 3.2 for other references.

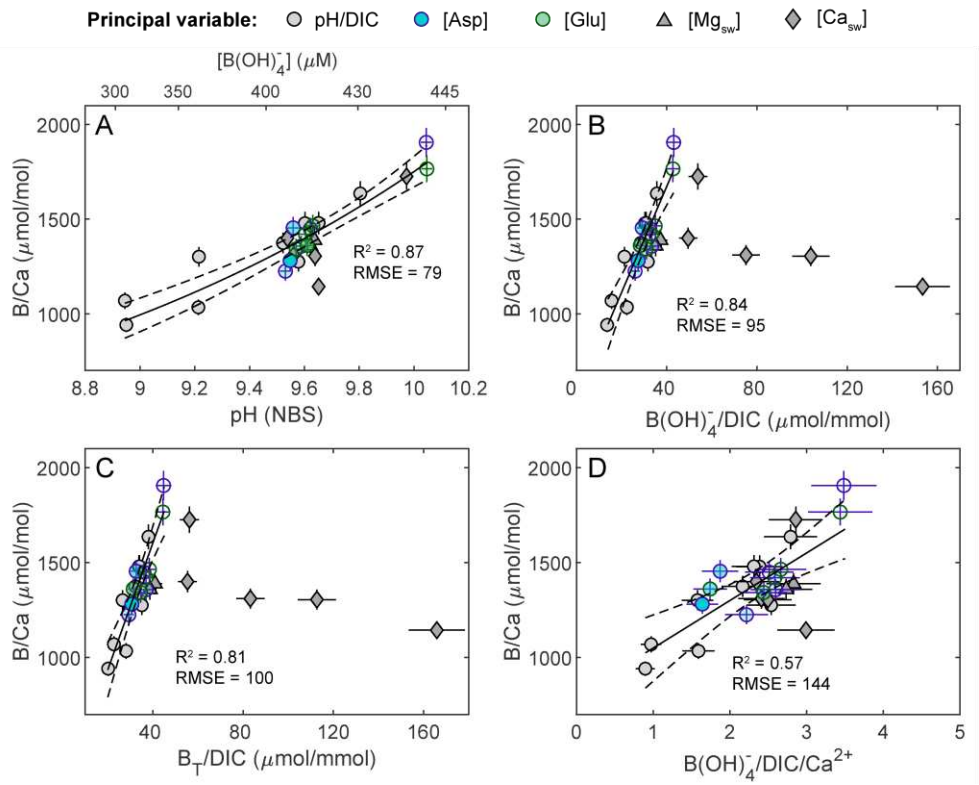

Fig. 7. Boron partitioning into ACC. Only data from precipitates which were unambiguously entirely ACC are shown (see text). (A) B/Ca as a function of pH. (B) B/Ca as a function of the seawater $B(OH)_4^-$/DIC ratio. $B(OH)_4^-$/DIC calculated using DIC measured at the end of precipitation is shown (Tab. S4), except in the case of the variable [Ca] and [Mg] experiments for which calculated DIC was used (Tab. 1), see Evans et al. (2019).(C) B/Ca as a function of the seawater total boron/DIC ratio. Although ACC B/Ca is marginally better described by the seawater $B(OH)_4^-$/DIC ratio we cannot identify whether $B(OH)_4^-$ is the only species incorporated into ACC based on these data because pH and DIC broadly unavoidably covaried in our experiments. (D) As in panel C, except further normalised to seawater Ca^{2+}. In panels B and C, the regression only considers data from ACCs precipitated from seawater with a [Ca^{2+}] close to natural (>4), whereas all data are considered in panel D. Error estimates propagate the uncertainty in DIC, variation in pH during the titration, and electrode-derived [Ca^{2+}] precision (where relevant).

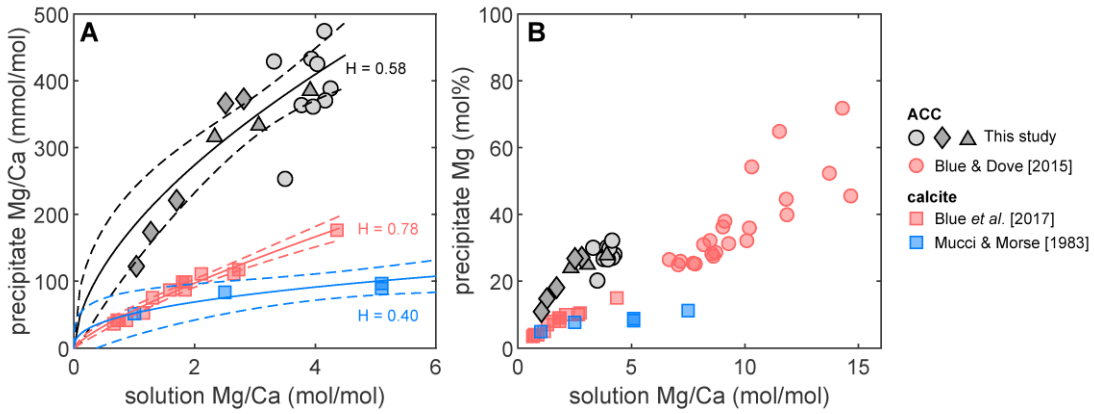

Fig. 8. Mg incorporation into ACC precipitated from seawater as a function of the solution Mg/Ca ratio. (A) Compared to calcite resulting from the transformation of ACC in $MgCl_2$-$CaCl_2$-$NaHCO_3$ solutions (Blue et al., 2017) and calcite precipitated from seawater (Mucci and Morse, 1983). H-values refer to the power coefficient of the least-squares regressions. (B) Compared to ACC precipitated from $MgCl_2$-$CaCl_2$-$NaHCO_3$/Na_2CO_3 solutions and at higher solution Mg/Ca ratios (Blue and Dove, 2015).

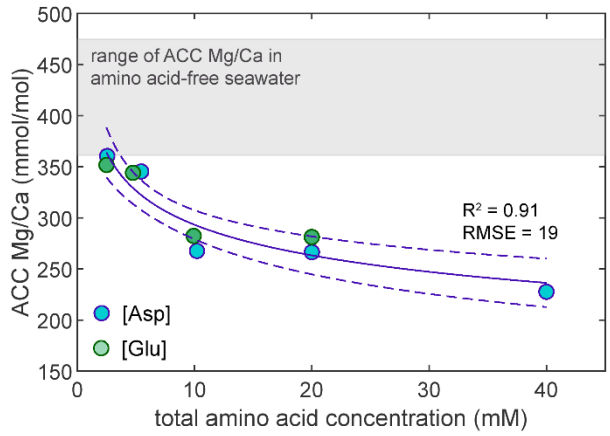

Fig. 9. ACC Mg/Ca ratio as a function of the seawater amino acid concentration. The presence of both aspartic and glutamic acid result in significantly reduced ACC Mg/Ca at amino acid concentrations >~2 mM, as expected given the preferential affinity for these amino acids to form ligands with Mg compared to Ca in solution (cf. Wang et al., 2009).

Tab. 1. Seawater chemistry conditions and titration details, resulting precipitate element/Ca ratios, and calculated distribution coefficients. Experiments were conducted from three different seawater reservoirs, made according to the same recipe but with minor differences in their trace element composition (see the supplementary material for full characterisation). Trace element ratios are given in μmol mol^{-1} in the case of Li/Ca, B/Ca, Mn/Ca, and Ba/Ca, mmol mol^{-1} in the case of Na/Ca, Mg/Ca and Sr/Ca, and nmol mol^{-1} in the case of U/Ca. D_B and D_U are calculated using (e.g.) the seawater B/Ca ratio for consistency, but especially in the case of boron are more appropriately described as a function of the seawater carbonate system (see the text and supplementary material for an exploration of this).

principal variable	pH (NBS)	DIC (μM)	titration rate (ml/min)	seawater [Ca] (mM)	seawater [Mg] (mM)	seawater reservoir	AA conc. (mM)	Li/Ca	B/Ca	Na/Ca	Mg/Ca	Mn/Ca	Sr/Ca	Ba/Ca	U/Ca	D_{Li} ($\times 10^{-3}$)	D_B	D_{Na} ($\times 10^{-3}$)	D_{Mg}	D_{Mn}	D_{Sr}	D_{Ba}	D_U
pH/DIC	9.21	17750	0.5	14.0	53.0	1		3.14	1034	64.5	363.6	127	4.47	492	132	1.12	0.032	1.86	0.096	27.0	0.68	2.09	0.12
	9.58	14164	0.5	12.5	53.0	1		6.39	1275	67.0	388.5	178	4.51	488	150	2.02	0.035	1.72	0.091	33.8	0.61	1.84	0.12
	10.08	9953	0.5	14.3	53.0	1		3.71	2197	70.4	568.5	627	4.25	451	236	1.34	0.068	2.06	0.153	135.8	0.66	1.94	0.22
	8.95	24848	0.5	15.1	53.0	1		4.10	941	67.3	253.2	102	4.06	514	122	1.57	0.031	2.09	0.072	23.5	0.67	2.35	0.12
	9.60	14430	0.2	12.7	53.0	1		3.14	1479	60.9	370.6	186	4.57	478	145	1.01	0.041	1.60	0.089	36.0	0.63	1.84	0.12
	9.60	13075	1.0	13.4	53.0	1		3.31	1480	60.4	361.4	182	4.59	483	147	1.12	0.043	1.66	0.091	36.9	0.66	1.95	0.13
	8.95	21639	0.5	16.0	53.0	1		4.72	1069	91.2	429.0	80	5.24	364	109	1.91	0.037	2.99	0.129	19.3	0.91	1.76	0.12
	9.22	18119	0.5	13.5	53.0	1		6.24	1301	125.2	433.0	124	5.22	384	123	2.13	0.038	3.47	0.110	25.4	0.76	1.56	0.11
	9.52	14789	0.5	13.2	53.0	1		5.16	1374	81.2	425.3	156	5.11	416	125	1.72	0.039	2.20	0.105	31.1	0.73	1.65	0.11
	9.80	12414	0.5	12.8	53.0	1		3.88	1636	59.2	474.4	257	5.01	418	131	1.25	0.045	1.56	0.114	49.9	0.69	1.61	0.11
	10.11	9739	0.5	12.1	53.0	1		2.13	1999	28.1	679.8	991	4.99	374	185	0.65	0.053	0.70	0.155	182.1	0.65	1.37	0.15
[Mg]	9.66	9639	0.5	13.0	30.0	2		4.52	1176	58.4	315.7	165	5.94	270	111	1.31	0.032	1.60	0.135	27.3	0.77	0.72	0.09
	9.64	11804	0.5	13.2	40.0	2		3.78	1388	43.5	333.0	210	5.49	297	127	1.11	0.038	1.19	0.109	35.2	0.72	0.81	0.10
	9.62	12489	0.5	12.9	50.0	2		3.50	1359	44.2	385.1	185	5.27	316	127	1.00	0.036	1.17	0.098	30.2	0.68	0.84	0.10
[Ca]	9.97	8177	0.5	18.8	53.0	1		5.47	1726	92.6	373.0	233	3.34	544	308	2.61	0.071	3.57	0.133	66.7	0.68	3.10	0.38
	10.09	4176	0.5	46.1	53.0	1		2.11	2331	44.0	254.4	416	1.53	428	307	2.46	0.234	4.06	0.221	291.8	0.76	5.97	0.94
	9.54	8734	0.5	21.1	53.0	2		3.33	1400	45.0	366.3	129	3.74	336	130	1.57	0.061	1.94	0.146	34.6	0.79	1.46	0.17
	9.56	5809	0.5	31.2	53.0	2		9.51	1310	34.3	221.1	119	2.45	358	193	6.61	0.084	2.16	0.130	47.1	0.76	2.31	0.37
	9.64	4289	0.5	41.7	53.0	2		6.15	1305	31.0	173.4	135	1.92	366	170	5.71	0.112	2.60	0.136	71.5	0.80	3.15	0.44
	9.65	2914	0.5	51.3	53.0	2		8.86	1144	24.1	122.3	241	1.54	409	215	10.13	0.121	2.46	0.118	157.4	0.79	4.34	0.68
[Asp]	10.05	11057	0.5	12.4	53.0	1	2.5	4.12	1906	87.7	504.2	447	4.29	467	216	1.29	0.051	2.23	0.118	83.9	0.57	1.74	0.18
	9.64	-	0.5	-	53.0	1	2.6	3.25	1449	41.4	360.4	140	5.02	487	135	-	-	-	-	-	-	-	-
	9.59	12474	0.5	12.8	53.0	2	5.4	3.59	1357	50.1	345.2	137	5.08	336	142	1.03	0.036	1.32	0.084	22.3	0.65	0.89	0.11
	9.53	13364	0.5	11.7	53.0	1	10.2	3.52	1225	46.9	267.5	91	4.88	473	133	1.05	0.031	1.13	0.059	16.3	0.62	1.68	0.10
	9.56	15264	0.5	15.6	53.0	1	20.0	-	1454	62.1	266.3	75	4.09	476	141	-	0.049	1.98	0.078	17.7	0.69	2.24	0.15
Asp+Glu	9.55	16375	0.5	16.7	53.0	1	40.0	4.58	1281	69.4	227.5	55	4.01	492	112	1.93	0.046	2.37	0.072	14.0	0.72	2.48	0.12
[Glu]	10.05	11138	0.5	12.4	53.0	1	2.0	2.87	1766	69.2	582.9	483	4.43	427	205	0.91	0.048	1.77	0.137	91.3	0.60	1.60	0.17
	9.63	12744	0.5	13.1	53.0	2	2.5	2.77	1464	40.1	351.6	188	4.98	342	146	0.81	0.040	1.08	0.087	31.4	0.65	0.93	0.12
	9.60	13519	0.5	12.9	53.0	2	4.7	2.89	1420	41.5	343.9	168	5.02	338	141	0.83	0.038	1.10	0.084	27.5	0.65	0.90	0.11
	9.57	14324	0.5	12.7	53.0	2	9.9	3.42	1342	45.0	282.2	143	4.78	353	135	0.97	0.035	1.18	0.068	23.2	0.61	0.93	0.11
	9.61	15933	0.5	16.2	53.0	1	20.0	3.22	1361	69.1	281.1	110	3.97	468	139	1.32	0.048	2.30	0.086	27.0	0.70	2.29	0.15
calcites or	9.58	-	0.5	10.3	0.1	3		19.79	2474	28.2	0.1	7	1.65	422	231	5.16	0.055	0.60	0.014	1.0	0.18	1.31	0.16
calcite/ACC	10.01	4504	0.5	-	5.0	3		49.50	536	40.1	21.2	12	4.68	322	1	-	-	-	-	-	-	-	-
mixtures	9.76	11088	0.5	13.5	10.0	3		18.20	850	69.8	65.6	56	5.56	560	0	6.22	0.025	2.03	0.088	38.6	1.02	1.84	0.01
	9.85	5350	0.5	-	10.0	3		43.44	653	38.2	21.6	18	3.48	371	2	-	-	-	-	-	-	-	-
	9.58	6820	0.5	13.1	10.0	3		5.17	772	65.3	38.2	6	4.79	554	2	1.72	0.022	1.85	0.050	4.0	0.85	1.77	0.04
	9.72	-	0.5	-	10.0	3		44.94	569	39.4	33.8	28	3.88	342	1	-	-	-	-	-	-	-	-
	9.60	6289	0.5	11.7	10.3	3		44.51	633	33.7	29.6	35	3.98	144	247	11.56	0.015	0.85	0.033	5.2	0.46	0.35	0.18
	9.61	7994	0.5	12.4	20.3	3		52.64	407	25.1	76.1	69	4.15	212	488	14.50	0.010	0.66	0.046	10.8	0.51	0.54	0.37
brucites	10.36	8971	0.5	13.3	53.0	1		118.23	22770	1749.4	6339.6	781	3.81	441	6968	39.72	0.657	47.75	1.587	157.5	0.55	1.77	6.13
	10.21	-	0.5	-	53.0	1		17.22	26983	293.0	7823.4	1415	3.62	340	10130	-	-	-	-	-	-	-	-

References

Allison N., Cohen I., Finch A. a, Erez J. and Tudhope A. W. (2014) Corals concentrate dissolved inorganic carbon to facilitate calcification. *Nat. Commun.* **5**, 5741.

Andersen F. A. and Brečević L. (1991) Infrared spectra of amorphous and crystalline calcium carbonate. *Acta Chem. Scand.* **45**, 1018–1024.

Beniash E., Aizenberg J., Addadi L., Weiner S. and B P. R. S. L. (1997) Amorphous calcium carbonate transforms into calcite during sea urchin larval spicule growth Amorphous calcium carbonate transforms into calcite during sea urchin larval spicule growth. *Proc. R. Soc. London B* **264**, 461–465.

Bentov S., Brownlee C. and Erez J. (2009) The role of seawater endocytosis in the biomineralization process in calcareous foraminifera. *Proc. Natl. Acad. Sci. U. S. A.* **106**, 21500–4.

Bentov S. and Erez J. (2006) Impact of biomineralization processes on the Mg content of foraminiferal shells: A biological perspective. *Geochemistry Geophys. Geosystems* **7**.

Blue C. R. and Dove P. M. (2015) Chemical controls on the magnesium content of amorphous calcium carbonate. *Geochim. Cosmochim. Acta* **148**, 23–33.

Blue C. R., Giuffre A., Mergelsberg S., Han N., Yoreo J. J. De and Dove P. M. (2017) Chemical and physical controls on the transformation of amorphous calcium carbonate into crystalline CaCO 3 polymorphs. **196**, 179–196.

Branson O. (2018) Boron Incorporation into Marine CaCO3. In *Boron Isotopes. Advances in Isotope Geochemistry*. (eds. H. Marshall and G. Foster). Springer, Cham.

Brecevic L. and Nielsen A. E. (1989) Solubility of amorphous calcium carbonate. **98**, 504–510.

Burton E. A. and Walter L. M. (1991) The effects of Pc02 and temperature on ~ nesium incorpo ~ tion in calcite in seawater and MgC12-CaC12 solutions. **55**, 777–785.

Busenberg E. and Plummer L. N. (1986) The solubility of BaCO3(cr) (witherite) in CO2-H2O solutions between 0 and 90oC, evaluation of the association constants of BaHCO3 (aq) and BaCO3 (aq) between 5 and 80oC , and a preliminary evaluation of the thermodynamic properties of Ba2+ (aq). *Geochim. Cosmochim. Acta* **50**, 2225–2233.

Busenberg E. and Plummer L. N. (1984) The solubility of strontianite (SrCO3) in CO2-H2O solutions between 2 and 91oC, the association constants of STHCO3+(aq) and SrCO30(aq) between 5 and 80oC, and an evaluation of the thermodynamic properties of Sr2+(aq) and SrCO3 (cr) at 25oC and 1 atm tota. *Geochim. Cosmochim. Acta* **48**.

De Choudens-Sanchez V. and Gonzalez L. a. (2009) Calcite and Aragonite Precipitation Under Controlled Instantaneous Supersaturation: Elucidating the Role of CaCO3 Saturation State and Mg/Ca Ratio on Calcium Carbonate Polymorphism. *J. Sediment. Res.* **79**, 363–376.

Decarlo T. M., Gaetani G. A., Holcomb M. and Cohen A. L. (2015) Experimental determination of factors controlling U/Ca of aragonite precipitated from seawater : Implications for interpreting coral skeleton. *Geochim. Cosmochim. Acta* **162**, 151–165.

Decarlo T. M., Holcomb M. and McCulloch M. T. (2018) Reviews and syntheses: Revisiting the boron systematics of aragonite and their application to coral calcification. *Biogeosciences* **15**, 2819–2834.

DePaolo D. J. (2011) Surface kinetic model for isotopic and trace element fractionation during precipitation of calcite from aqueous solutions. *Geochim. Cosmochim. Acta* **75**, 1039–1056.

Dickson A. G. (1990) Thermodynamics of the dissociation of boric acid in synthetic seawater from 273.15 to 318.15 K. *Deep Sea Res.* **37**, 755–766.

Dickson A. G. and Millero F. J. (1987) A comparison of the equilibrium constants for the dissociation

of carbonic acid in seawater media. *Deep Sea Res.* **34**, 1733–1743.
Dietzel M., Gussone N. and Eisenhauer A. (2004) Co-precipitation of Sr2+ and Ba2+ with aragonite by membrane diffusion of CO2 between 10 and 50 °C. *Chem. Geol.* **203**, 139–151.
Erez J. (2003) The source of ions for biomineralization in foraminifera and their implications for paleoceanographic proxies (Review). *Rev. Mineral. geochemistry* **54**, 115.
Evans D., Erez J., Oron S. and Müller W. (2015) Mg/Ca-temperature and seawater-test chemistry relationships in the shallow-dwelling large benthic foraminifera Operculina ammonoides. *Geochim. Cosmochim. Acta* **148**, 325–342.
Evans D., Müller W. and Erez J. (2018) Assessing foraminifera biomineralisation models through trace element data of cultures under variable seawater chemistry. *Geochim. Cosmochim. Acta*.
Evans D., Webb P., Penkman K. E. H., Kroger R. and Allison N. (2019) The characteristics and biological relevance of inorganic amorphous calcium carbonate (ACC) precipitated from seawater. *Cryst. Growth Des.*
Füger A., Konrad F., Leis A., Dietzel M. and Mavromatis V. (2019) Effect of growth rate and pH on lithium incorporation in calcite. *Geochim. Cosmochim. Acta* **248**, 14–24.
Gagnon A. C., Adkins J. F. and Erez J. (2012) Seawater transport during coral biomineralization. *Earth Planet. Sci. Lett.* **329–330**, 150–161.
Giuffre A. J., Gagnon A. C., De Yoreo J. J. and Dove P. M. (2015) Isotopic tracer evidence for the amorphous calcium carbonate to calcite transformation by dissolution-reprecipitation. *Geochim. Cosmochim. Acta* **165**, 407–417.
Hain M. P., Sigman D. M., Higgins J. A. and Haug G. H. (2015) The effects of secular calcium and magnesium concentration changes on the thermodynamics of seawater acid/base chemistry: Implications for Eocene and Cretaceous ocean carbon chemistry and buffering. *Glob. Biogeochem. Cycles* **29**, 517–533.
Hauzer H., Evans D., Müller W., Rosenthal Y. and Erez J. (2018) Calibration of Na partitioning in the calcitic foraminifer Operculina ammonoides under variable Ca concentration: Toward reconstructing past seawater composition. *Earth Planet. Sci. Lett.* **497**, 80–91.
Holcomb M., DeCarlo T. M., Gaetani G. A. and McCulloch M. (2016) Factors affecting B/Ca ratios in synthetic aragonite. *Chem. Geol.* **437**, 67–76.
Ishikawa M. and Ichikuni M. (1984) Uptake of sodium and potassium by calcite. *Chem. Geol.* **42**, 137–146.
Jacob D. E., Wirth R., Agbaje O. B. A., Branson O. and Eggins S. M. (2017) Planktic foraminifera form their shells via metastable carbonate phases. *Nat. Commun.* **8**, 1–8.
Johnson K. S. (1982) Solubility of rhodochrosite (MnCO3) in water and seawater. *Geochim. Cosmochim. Acta* **46**, 1805–1809.
Keul N., Langer G., De Nooijer L. J., Nehrke G., Reichart G. J. and Bijma J. (2013) Incorporation of uranium in benthic foraminiferal calcite reflects seawater carbonate ion concentration. *Geochemistry, Geophys. Geosystems* **14**, 102–111.
Kim Y.-Y., Carloni J. D., Demarchi B., Sparks D., Reid D. G., Kunitake M. E., Tang C. C., Duer M. J., Freeman C. L., Pokroy B., Penkman K., Harding J. H., Estroff L. A., Baker S. P. and Meldrum F. C. (2016) Tuning hardness in calcite by incorporation of amino acids. *Nat. Mater.* **in press**, DOI: 10.1038/nmat4631.
King J. K. and Hare P. E. (1972) Amino acid composition of the test as a taxonomic character for living and fossil planktonic foraminifera. *Micropaleontology* **18**, 285–293.
Kitano Y., Kanamori N. and Oomori T. (1971) Measurement of distribution coefficients of strontium and barium between carbonate precipitate and solution - Abnormally high values of distribution

879 coefficients measured at early stages of carbonate formation. *Geochem. J.* **4**, 183–206.
880 Konrad F., Gallien F., Gerard D. E. and Dietzel M. (2016) Transformation of Amorphous Calcium
881 Carbonate in Air. *Cryst. Growth Des.* **16**, 6310–6317.
882 Lam R. S. K., Charnock J. M., Lennie A. and Meldrum F. C. (2007) Synthesis-dependant structural
883 variations in amorphous calcium carbonate. *CrystEngComm* **9**, 1226–1236.
884 Lewis E. and Wallace D. (1998) *Program developed for CO2 system calculations.*, Upton, New York.
885 Marriott C. S., Henderson G. M., Belshaw N. S. and Tudhope A. W. (2004) Temperature dependence
886 of δ7Li, δ44Ca and Li/Ca during growth of calcium carbonate. *Earth Planet. Sci. Lett.* **222**, 615–
887 624.
888 Mavromatis V., Goetschl K. E., Grengg C., Konrad F., Purgstaller B. and Dietzel M. (2018)
889 ScienceDirect Barium partitioning in calcite and aragonite as a function of growth rate. **237**, 65–
890 78.
891 McCulloch M. T., D'Olivo J. P., Falter J., Holcomb M. and Trotter J. A. (2017) Coral calcification in a
892 changing World and the interactive dynamics of pH and DIC upregulation. *Nat. Commun.* **8**, 1–
893 8.
894 Millero F. J. (2013) *Chemical Oceanography*. 4th ed., Taylor & Francis Group, Boca Raton.
895 Mucci A. (1988) Manganese uptake during calcite precipitation from seawater: Conditions leading to
896 the formation of a pseudokutnahorite. *Geochim. Cosmochim. Acta* **52**, 1859–1868.
897 Mucci A. and Morse J. W. (1983) The incorporation of Mg2+ and Sr2+ into calcite overgrowths:
898 influences of growth rate and solution composition. *Geochim. Cosmochim. Acta* **47**, 217–233.
899 Nehrke G., Reichart G. J., Van Cappellen P., Meile C. and Bijma J. (2007) Dependence of calcite
900 growth rate and Sr partitioning on solution stoichiometry: Non-Kossel crystal growth. *Geochim.*
901 *Cosmochim. Acta* **71**, 2240–2249.
902 de Nooijer L. J., Spero H. J., Erez J., Bijma J. and Reichart G. J. (2014) Biomineralization in perforate
903 foraminifera. *Earth-Science Rev.* **135**, 48–58.
904 de Nooijer L. J., Toyofuku T. and Kitazato H. (2009) Foraminifera promote calcification by elevating
905 their intracellular pH. *Proc. Natl. Acad. Sci. U. S. A.* **106**, 15374–15378.
906 Okumura M. and Kitano Y. (1986) Coprecipitation of alkali metal ions with calcium carbonate.
907 *Geochim. Cosmochim. Acta* **50**, 49–58.
908 Parkhurst D. L. and Appelo C. A. J. (1999) *User's Guide to PHREEQC — a Computer Program for*
909 *Speciation, Batch-Reaction, One-dimensional Transport, and Inverse Geochemical Calculations.*,
910 Politi B. Y., Levi-kalisman Y., Raz S., Wilt F., Addadi L., Weiner S. and Sagi I. (2006) Structural
911 Characterization of the Transient Amorphous Calcium Carbonate Precursor Phase in Sea
912 Urchin Embryos **. , 1289–1298.
913 Purgstaller B., Goetschl K. E., Mavromatis V. and Dietzel M. (2019) Solubility investigations in the
914 amorphous calcium magnesium carbonate system. *CrystEngComm* **21**, 155–164.
915 Reeder R. J., Elzinga E. J., Tait C. D., Rector K. D., Donohoe R. J. and Morris D. E. (2004) Site-specific
916 incorporation of uranyl carbonate species at the calcite surface. *Geochim. Cosmochim. Acta* **68**,
917 4799–4808.
918 Reeder R. J., Nugent M., Lamble G. M., Tait C. D. and Morris D. E. (2000) Uranyl incorporation into
919 calcite and aragonite: XAFS and luminescence studies. *Environ. Sci. Technol.* **34**, 638–644.
920 Sviben S., Gal A., Hood M. A., Bertinetti L., Politi Y., Bennet M., Krishnamoorthy P., Schertel A.,
921 Wirth R., Sorrentino A., Pereiro E., Faivre D. and Scheffel A. (2016) A vacuole-like compartment
922 concentrates a disordered calcium phase in a key coccolithophorid alga. *Nat. Commun.* **7**, 11228.
923 Uchikawa J., Penman D. E., Zachos J. C. and Zeebe R. E. (2015) Experimental evidence for kinetic
924 effects on B/Ca in synthetic calcite: Implications for potential B(OH)4- and B(OH)3

925 incorporation. *Geochim. Cosmochim. Acta* **150**, 171–191.
926 Wang D., Wallace A. F., De Yoreo J. J. and Dove P. M. (2009) Carboxylated molecules regulate
927 magnesium content of amorphous calcium carbonates during calcification. *Proc. Natl. Acad. Sci.*
928 *U. S. A.* **106**, 21511–6.
929 Watson E. B. (2004) A conceptual model for near-surface kinetic controls on the trace- element and
930 stable isotope composition of abiogenic calcite crystals. *Geochim. Cosmochim. Acta* **68**, 1473–
931 1488.
932 Weremeichik J. M., Gabitov R. I., Thien B. M. J. and Sadekov A. (2017) The effect of growth rate on
933 uranium partitioning between individual calcite crystals and fluid. *Chem. Geol.* **450**, 145–153.
934 White A. F. (1977) Sodium and potassium coprecipitation in aragonite. *Geochim. Cosmochim. Acta*
935 **41**, 613–625.
936 White A. F. (1978) Sodium coprecipitation in calcite and dolomite. *Chem. Geol.* **23**, 65–72.
937 Wolthers M., Nehrke G., Gustafsson J. P. and Van Cappellen P. (2012) Calcite growth kinetics:
938 Modeling the effect of solution stoichiometry. *Geochim. Cosmochim. Acta* **77**, 121–134.
939